Catena 260 (2025) 109450

Contents lists available at ScienceDirect

Catena

journal homepage: www.elsevier.com/locate/catena

Squeeze of Brazilian subtropical mangroves from a Holocene and Anthropocene perspective

Marcelo C.L. Cohen [a,b,*], Neuza A. Fontes [a], Erika Rodrigues [a], Luiz C.R. Pessenda [c], Marlon Carlos França [d], Ed Garrett [e], Junghyung Ryu [f,**]

[a] Graduate Program of Geology and Geochemistry, Federal University of Pará. Av. Perimentral 2651, Terra Firme, 66077-530, Belém, (PA), Brazil
[b] Department of Oceanography and Coastal Sciences, Louisiana State University, Baton Rouge, LA 70803, USA
[c] University of São Paulo, CENA/^{14}C Laboratory, Av. Centenário 303, 13400-000, Piracicaba, São Paulo, Brazil
[d] Laboratory of Oceanography and Climate, Federal Institute of Espírito Santo, Rua Augusto Costa de Oliveira, 660, Centro, 29285-000, Piúma, (ES), Brazil
[e] Department of Environment and Geography, University of York, Wentworth Way, Heslington, York YO10 5NG, United Kingdom
[f] Division of Earth and Environmental System Sciences, Department of Oceanography, Pukyong National University, Yongso-ro, Nam-gu, 48513 Busan, Republic of Korea

ARTICLE INFO

Keywords:
Anthropocene
Coastal area
Drone
Global warming
Little Ice Age
Rhizophora

ABSTRACT

Globally, mangroves are expected to expand into subtropical latitudes and higher elevations due to rising temperatures and sea-level over the coming decades. However, local geomorphology and coastal urbanization may strongly modulate these responses. Insights into mangrove responses to environmental changes can be gained from the last millennium, a key period marking the transition from natural to anthropogenic influence. Remote sensing and multi-proxy analyses from a subtropical Brazilian coast revealed the presence of mangroves on elevated flats (>1.5 m above mean sea level, msl) around ~1700 cal yr BP. These mangroves migrated to lower flats (~70 cm below current msl) by ~530 cal yr BP (1420 CE), in response to a relative sea-level (RSL) fall. This trend contrasts with the RSL rise since the end of the Little Ice Age (LIA, ~1300–1850 CE), which has since driven landward mangrove migration in the area. Additionally, recent warming in South America has facilitated the poleward expansion of *Rhizophora* species, contributing to an increase in mangrove canopy height (from 1 to 3.5 m) over recent decades. While global warming favors latitudinal expansion and canopy growth, the availability of suitable land is critical. Elevated terraces, which served as refuges for coastal wetlands during the mid-Holocene high sea-level stand, are now urbanized, limiting future establishment. Thus, mangrove expansion into temperate latitudes and landward migration hinge on horizontal space availability and the degree of urban development. Gentle terrain (slopes of 1.3–0.8 %) supports mangrove persistence, while steep slopes (>14 %) and urban encroachment threaten their survival. Without adequate space for migration, the region may face a net mangrove loss—termed "mangrove squeeze"—between 2100 and 2160 CE.

1. Introduction

Globally, rates of mean sea-level rise have increased progressively from 1.1 mm/yr (1902 to 1990, Dangendorf et al., 2017) to ~4.5 mm/yr in 2023 (Hamlington et al., 2024) and these rates are expected to accelerate to between ~5 mm/yr (low CO_2 emissions scenario) and ~10 mm/yr (high emissions scenario) by 2100 (Kopp et al., 2014). Projections of sea-level rise have revealed scenarios from 38 (SSP1-1.9) to 77 cm (SSP5-8.5) by 2100 (Fox-Kemper et al., 2021), and mangroves can likely not keep pace with RSL rise rates exceeding 6–10 mm/yr (Saintilan et al., 2020; Xie et al., 2022). To escape drowning, mangroves will migrate to higher surfaces, but coastal urbanization can be a physical barrier to inland mangrove migration (Leo et al., 2019). Then, these current rates and projections of sea-level rise have raised concerns about the survival of mangroves up to the end of this century. Spencer et al. (2016) estimate that a sea-level rise of 110 cm by 2100 would lead to the loss (392–578 × 10^3 km^2) of coastal wetlands worldwide. However, paleoecological studies have shown the resilience of mangroves in the face of high rates of early Holocene sea level rise (6–12 mm/yr, (Cronin, 2012) along a pristine Brazilian coast (Cohen et al., 2021, 2020a, 2012, 2005b; França et al., 2015). Mid-Holocene (~5500 cal yr BP) high sea-level stand reached up to 5 m above the current RSL, which

* Corresponding author at: Federal University of Pará – Brazil, Rua Augusto Corrêa, 01 - Guamá. CEP 66075-110, Belém, (PA), Brazil.
** Corresponding author at: Pukyong National University, Yongso-ro, Nam-gu, 48513, Busan, Republic of Korea.
E-mail addresses: mcohen@ufpa.br (M.C.L. Cohen), jryu@pknu.ac.kr (J. Ryu).

https://doi.org/10.1016/j.catena.2025.109450
Received 25 May 2025; Received in revised form 2 September 2025; Accepted 9 September 2025
Available online 22 September 2025

was followed by a fall along the Brazilian coast (Angulo et al., 2006; Angulo and Lessa, 1997; Boski et al., 2015; Cohen et al., 2021, 2020a; Toniolo et al., 2020), causing a landward followed by a seaward mangrove migration (Castro et al., 2013; Cohen et al., 2021, 2020a, 2012; Cohen et al., 2014; França et al., 2013; Lorente et al., 2014). Regarding the last centuries, the LIA (~1300 to 1850 CE, Lean and Rind (1999)) caused a minimum sea-level between −19 and −26 cm globally in 1730 CE (Grinsted et al., 2009). Multi-proxy studies in northern and northeastern Brazil indicated a landward mangrove migration since the end of the LIA event due to a RSL rise (Bozi et al., 2021; Cohen et al., 2005a).

In addition, global warming is driving a poleward shift of isotherms at an average rate of 27 km per decade (Burrows et al., 2011), resulting in a northward mangrove expansion (Cavanaugh et al., 2014; Osland et al., 2021, 2018, 2017; Osland and Feher, 2020; Perry and Mendelssohn, 2009; Rodrigues et al., 2021; Saintilan et al., 2014). Cold temperatures have restricted the northern limits of American mangroves to ~30° N (Kangas et al., 1961; Rodrigues et al., 2021; Yao et al., 2022). The southern boundary of American mangroves could also be migrating southward (Cohen et al., 2020b; Rodrigues et al., 2022), because the minimum temperatures annually (+0.5 °C per decade) and in winter (+0.4 °C per decade) have increased in Southern Brazil between 1960 and 2002 (Marengo and Camargo, 2008), with projections between + 3 and + 5°C by 2080 (Marengo, 2006). Supposing this recent temperature rise is inducing such poleward mangrove migration, *Rhizophora*, which is less tolerant to low winter temperatures among the mangrove genera (Stuart et al., 2007), should be invading subtropical mangroves with *Laguncularia* and *Avicennia*, followed by a mangrove expansion on higher surfaces due to sea-level rise.

Therefore, climate change may affect mangroves primarily through air warming, resulting in a mangrove expansion into temperate zones, whereas sea-level rise could result in losses of mangrove areas. Given these contrasting effects, will global warming lead to an expansion or contraction of subtropical mangroves? To answer this scientific question, this study aims to develop a paleoenvironmental reconstruction on both millennial and decadal scales, using satellite/drone images and

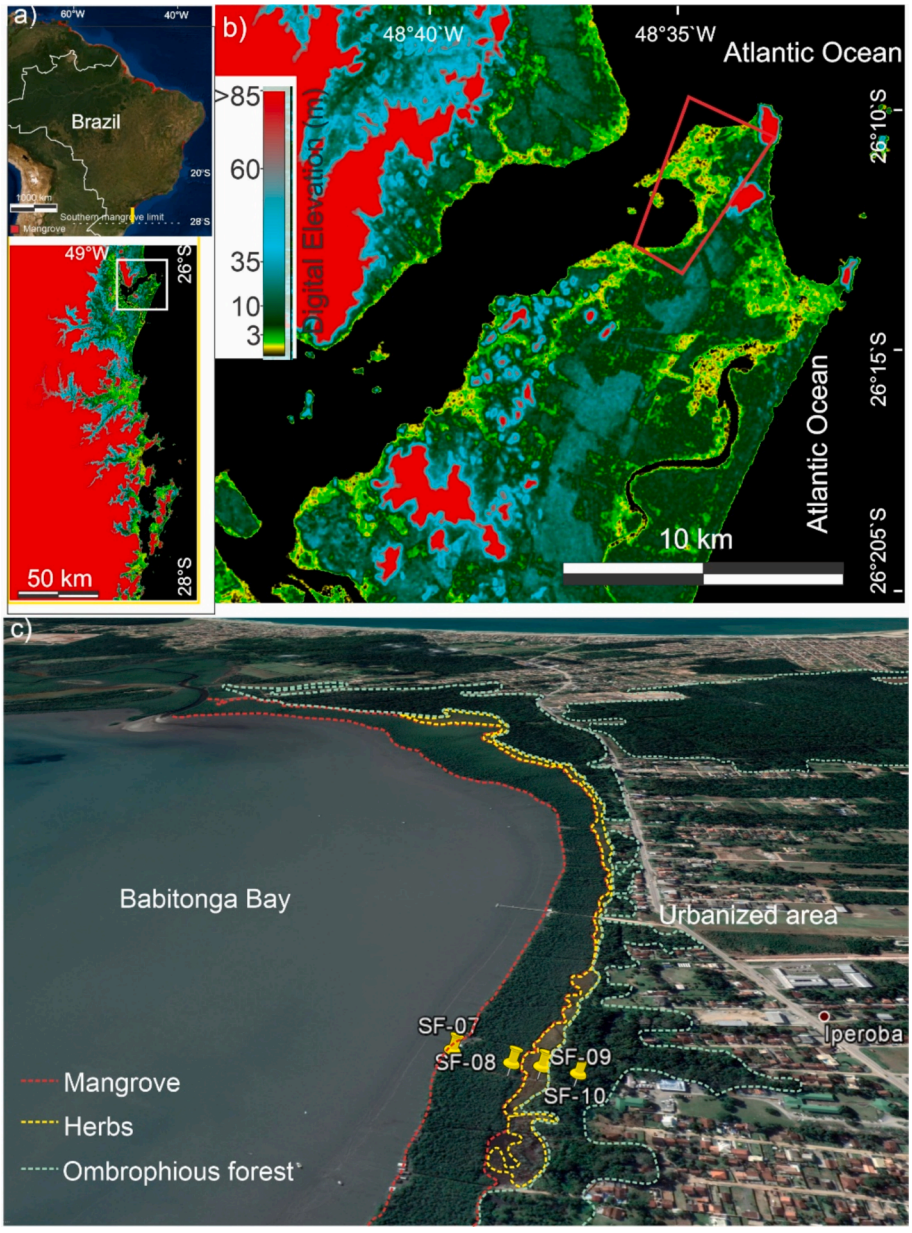

Fig. 1. A) Location of the study area and the southern American mangrove limit. b) Digital elevation model based on SRTM data of the study area. c) Satellite image showing the coastal vegetation zonation, urbanized zone and sampling core sites.

pollen data, geochemical ($\delta^{13}C$ and C\N) and sedimentary data, as well as ^{14}C dating along four cores sampled from coastal plain occupied by mangroves, herbaceous vegetation and ombrophilous forests, following a topographic gradient, near the austral mangrove limit. The coastal plain studied is between hills and elevated terraces where coastal urbanization is developed (Fig. 1), imposing physical barriers for natural inland mangrove migration. The results of this study, which represent the coastal morphology of southern Brazil, are essential for understanding the vulnerability of mangroves and anticipating the future of this important ecosystem in the face of climate and sea-level changes.

2. Modern settings

2.1. Study area

The study site is located at Babitonga Bay (26°12′49.53″S/48°35′8.29″W), State of Santa Catarina (Fig. 1). The city of Joinville borders the bay—one of the largest industrial and urban centers in southern Brazil—as well as other expanding municipalities such as São Francisco do Sul, Itapoá, and Araquari. Around Babitonga Bay, there is a population of approximately 700,000 inhabitants. Over recent decades, the region has experienced accelerated coastal urbanization, port expansion, and industrial development, leading to significant anthropogenic pressures on coastal ecosystems, including mangroves and estuarine wetlands. These pressures include land reclamation, pollution, habitat fragmentation, and modifications of hydrological regimes (Pinto et al., 2019). Despite these impacts, Babitonga Bay still retains extensive mangrove forests (~59 km^2) on microtidal flats (tidal range below 2 m), where the southern limit of *Rhizophora mangle* occurs, which is less adapted to low temperatures (Stuart et al., 2007) (Fig. 1a). Brazilian mangroves are distributed between the northern coast (04°20′N, Amapá State), with the three mangrove species (*Rhizophora mangle, Avicennia germinans,* and *Laguncularia racemosa*), and the southern coast (28°30′S, State of Santa Catarina), with *Avicennia germinans and Laguncularia racemosa,* the most cold-tolerant mangrove types (Cohen et al., 2020b; Schaeffer-Novelli et al., 2000). The bay has been influenced by the Cachoeira (drainage area of 80 km^2), Palmital (360 km^2), Cubatão (485 km^2), and Parati (70 km^2) rivers (Barros et al., 2010). The interaction between the Holocene sea-level changes and longshore sediment transport has modeled the bays, lagoons, or estuarine inlets (Angulo et al., 1999; Lessa et al., 2000; Zular et al., 2018). The bay presents Pleistocene and Holocene barriers with muddy tidal flats, beaches, beach ridges, and parabolic dunes (Zular et al., 2018).

2.2. Climatic and oceanographic setting

The climate of the study area is affected by a subtropical climate with wet summers (November to April) and moderately dry winters (May to October), with rainfall from 1600 to 1900 mm/yr and annual mean temperatures from 18 to 20 °C (Cfa, according to Koppen's classification) (Alvares et al., 2013). Tropical and extratropical atmospheric systems have controlled incursions of cold fronts related to polar air masses in southern Brazil (Nobre et al., 1986; Seluchi and Marengo, 2000)). Babitonga Bay is wave-dominated with semidiurnal microtides (0.8–1.5 m) and water salinities between 5.8 and 24 (Cunha et al., 2005; Mazzer and Gonçalves, 2011; Salles, 2000).

2.3. Vegetation

Tropical ombrophilous forest occupies the coastal terraces (Veloso et al., 1991), mainly represented by Anacardiaceae (e.g., *Tapirira guianensis*), Arecaceae (e.g., *Euterpe edulis*), Asteraceae (e.g., *Vernonanthura montevidensis*), Bignoniaceae (e.g., *Jacaranda puberula*), Euphorbiaceae (e.g., *Aparisthmium cordatum*), Fabaceae (e.g., *Schizolobium parahyba*), Melastomataceae (e.g., *Tibouchina mutabilis*), Myrtaceae (e.g., *Eugenia uniflora*, *Marlierea tomentosa,* Rubiaceae (e.g., *Psychotria* spp.) and Urticaceae (e.g., *Cecropia catarinenses*). Restinga vegetation occurs along the coastal plain mainly on dunes and is mainly represented by Asteraceae (e.g., *Baccharis singularis*), Bromeliaceae (e.g., *Aechmea gamosepala*), Fabaceae (e.g., *Dalbergia ecastaphyllum*), Rubiaceae (e.g., *Psychotria*) and Poaceae (e.g., *Lasiacis ligulata*). Mangroves, represented by *Rhizophora mangle*, *Laguncularia racemosa* and *Avicennia germinans* are colonizing the intertidal flats, while herbaceous vegetation, mainly characterized by Cyperaceae (e.g., *Schoenoplectus tabernaemontani*), Polypodiaceae (e.g., *Acrostichum aureum*) and Ruppiaceae (e.g., *Ruppia maritima*) occur on the highest tidal flats (Cunha et al., 2005).

3. Materials and methods

The process was carried out in four phases (Fig. 2): 1) Identification of mangroves in Babitonga Bay using satellite images; 2) Analysis of structural characteristics (density, tree height, and diameter at breast height), topographic measure using Theodolite/RTK-GNSS data, drone photogrammetry (2017 and 2024), and planialtimetric temporal analysis of mangroves; 3) Multi-proxy analysis; and 4) Combined surface

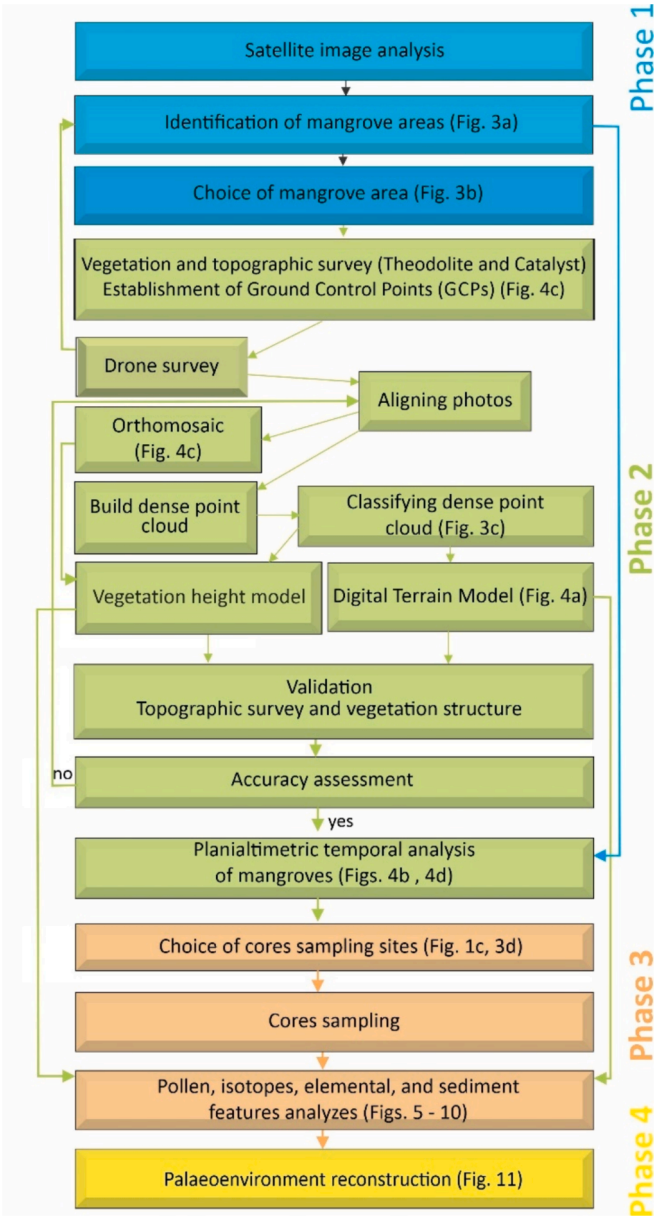

Fig. 2. Methodology flow modified from Cohen et al. (2023).

(satellite and drone) and subsurface (cores) data analysis for palaeoenvironmental reconstruction. Fig 3.

3.1. Satellite image data

QuickBird satellite images (Nov/2006), obtained from Google Earth (resolution of 2.44 m multispectral) were processed using Global Mapper version 25.1 to identify and quantify mangroves in Babitonga Bay. The vegetation cover categorization in the QuickBird images was primarily performed through visual classification in Global Mapper based on a dataset with identified land cover types, which were used to determine the image features corresponding to each land cover. Data assembly for training and testing focused primarily on various image characteristics. The "Create Area Features from Equal Values" tool enabled the conversion of raster to vector data or elevation grid to vector, based on pixel values. The image was divided using spectral, physical, and geometric parameters. To identify the multispectral digital numbers most representative of the mangroves, a matching threshold was set, where a value of zero indicated an exact match, and 256 encompassed the entire valid spectral range. This dataset allowed the identification of objects, which were then compared to a visual classification of drone orthoimages (2.6 cm/pixel) from 2017. The drone images enabled the differentiation of mangrove trees from herbaceous vegetation and ombrophilous forest. These images provided a dependable reference base for validating the classification derived from the QuickBird images. A visual inspection was then conducted to verify the classification of each mangrove unit in the QuickBird data. Further details on drone image processing can be found in (Cohen et al., 2020a; Cohen et al., 2018).

3.2. Drone data

High-resolution images acquired with a DJI Phantom 4 Advanced Drone, a Quadricopter equipped with GPS and inertial measurement systems, enabled the identification of coastal vegetation zonation. It features an FC 6310 digital 4 K/20MP (RGB) camera with a focal length of 8.8 mm and a sensor width of 12.8 mm, producing images with a width of 5472 pixels. The camera mounted on a motion-compensated gimbal, captured high spatial resolution images with a resolution of 2.6 cm/pixel (at a flight height of 100 m) for the study area. This spatial resolution was determined by the equation 1:

$$(1)\quad GSD = (Sw * H * 100/60) / (Fr * imH),$$

GSD represents the Ground Sampling Distance (in centimeters per pixel), *Sw* is the sensor width of the camera (in millimeters), *H* denotes the flight height (in meters), Fr refers to the focal length of the camera (in millimeters), and *imH* stands for the image width in pixels (PIX4D, 2013). The drone survey was conducted using DJI Ground Station Pro Software installed on a tablet, with predetermined missions. These missions followed a route defined by several navigation waypoints, with a 90° camera angle, 90 % frontal overlap, and 75 % lateral overlap. A total of five missions (2147 images) were flown in August 2017 (winter), covering 225 ha. A single mission was carried out in every designated mangrove area, with interruptions for replacing drone batteries. Each battery enabled scanning of ~48 ha (17–20 min of flight time).

3.3. Ground control points

Fieldwork was conducted in January 2017 to collect planialtimetric data using a Trimble Catalyst antenna equipped with a Differential Global Navigation Satellite System (GNSS) with a sub-meter correction. After a 30-minute stabilization period, the altimetric accuracy of the base station was determined to be ± 20 cm. Due to the extended stabilization time of the Catalyst antenna, the planialtimetric data collected with the Catalyst served as reference points for the topographic survey conducted with an electronic theodolite (model CST Berger DGT10). Once a planialtimetric reference point was set using the Catalyst, the theodolite was set up to measure the relative elevation for the Ground Control Points (GCPs). The planimetric data (±30 cm) and altimetric data (±10 cm) for the GCPs were obtained using the Catalyst and theodolite, respectively. The Geoidal Undulation Interpolation System (SIRGAS2000) from IBGE was used to convert ellipsoidal heights to orthometric heights. These data (20 points) were then used as GCPs to calibrate the Digital Surface Model (DSM) generated through photogrammetry. Vegetation heights (VH) were measured for mangrove and saltmarsh vegetation using a 4-meter ruler. Four 10x10 meter plots were established to assess the density, height, and diameter at the breast height of mangrove trees. These measurements were used to validate the vegetation height model derived from photogrammetry.

3.4. 3D models generation and validation

Images obtained by drone were processed using Agisoft Metashape Professional version 2.2.0 software. It generated 3D spatial data and orthomosaics with the assistance of ground control points (https://www.agisoft.com). Orthomosaic images from Aug/2017 and Jun/2024 were used in the time series analysis. A high-resolution dense point cloud (with point spacing ranging from 3 to 5 cm) was generated to create digital models of the surface, terrain, and vegetation. This process initially produced a digital surface model (DSM), which captured both natural elements (such as trees, herbs, sediments, soils, and water) and man-made structures (including power lines, buildings, and towers). A classification of the dense point cloud (DPC) was carried out to identify the terrain elevation. The resulting digital terrain model (DTM) focuses solely on the substrate surface, excluding vegetation and constructed features. The DPC was divided into cells, with the points in each cell being identified. Triangulating these points provided the initial estimate of the DTM. Additional points were incorporated into the DTM based on specific criteria: they needed to be within a specified distance from the terrain model, and the angle formed between the terrain model and a line connecting the new points had to be smaller than a predefined threshold. For nearly flat terrain, a default angle of 15 degrees is recommended, though a higher value should be used for terrain with steeper slopes (AgisoftPhotoScan, 2024). This method was applied to tidal flats with and without vegetation, including areas with mangrove and marsh vegetation. The significant elevation differences within the point clouds allowed for distinguishing points that represented vegetation from those indicating the substrate surface. A mesh representing the soil surface was then constructed, using only points that corresponded to the topographic surface. This process extended the topographic gradients from unvegetated or sparsely vegetated tidal flats to those with dense vegetation. The model was calibrated with ground control points (GCPs) obtained using a Trimble Catalyst DA2 and theodolite in areas with dense vegetation cover. As a result, the digital terrain model (DTM) beneath the vegetation cover was created by combining the GCP interpolation from vegetated flats with the topographic gradients of unvegetated flats extrapolated into vegetated areas. Accurate topographic surveys of tidal flats covered by dense mangroves are challenging due to the dense vegetation. Vector data containing elevation components were used to create an elevation grid through triangulation, employing a triangulated irregular network (TIN) that connects known elevation values. The vegetation height model was derived using the Combine/Compare Terrain Layers tool, which generates a new gridded elevation layer by combining or comparing two existing layers. This technique, for instance, was applied to subtract the gridded elevation layer representing the DSM from the DTM, producing the digital vegetation height model (DVHM). A quantitative analysis was then performed on the vertical differences between the checkpoints and the DTM and DVHM for 2017 and 2024 was performed using the equation proposed by (Cohen et al., 2018).

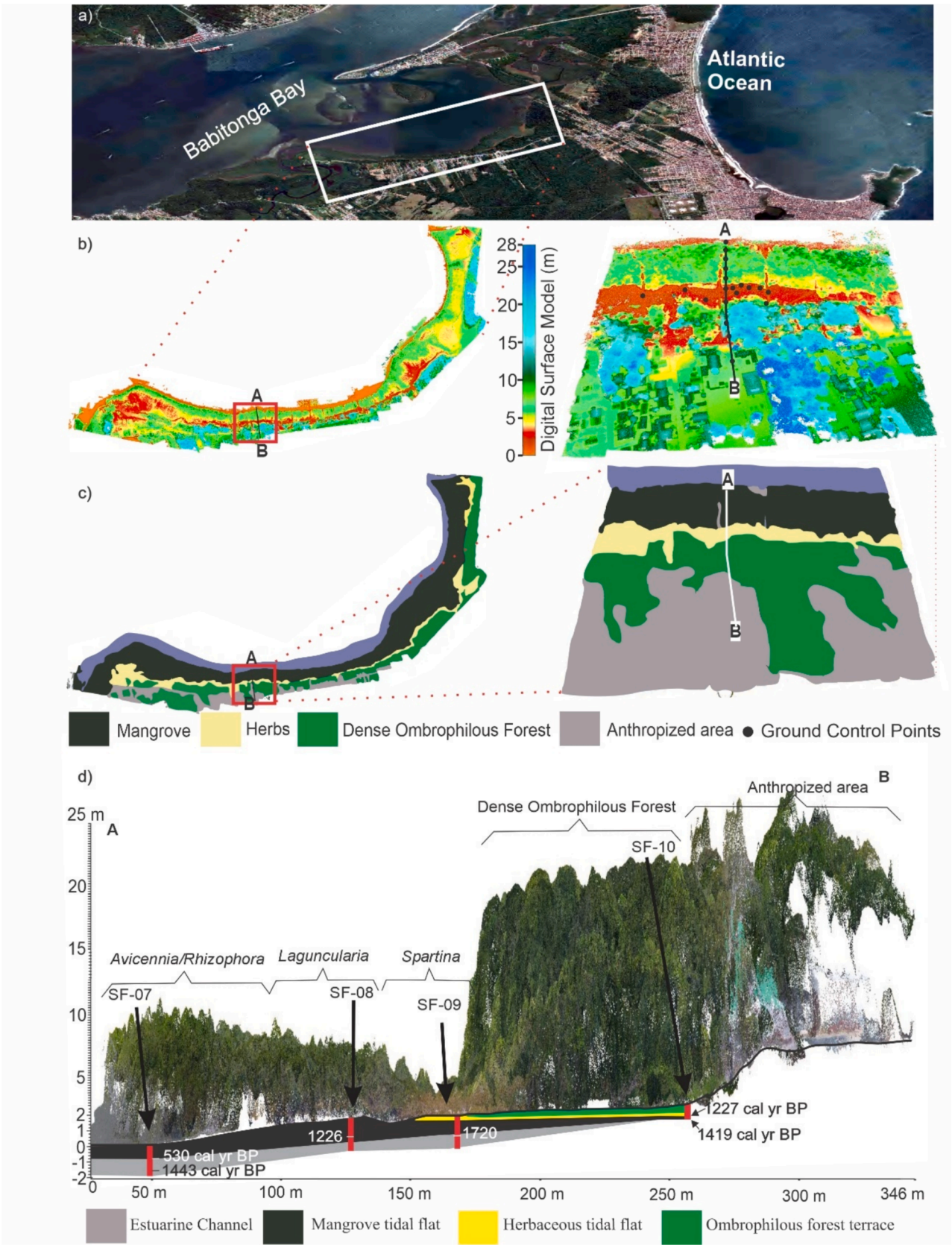

Fig. 3. A) Satellite image indicating the study area at babitonga bay. b) Digital elevation models highlighting the studied transect. c) Vegetation map for the study area. d) Elevation transect indicating the topography, vegetation canopy height and the facies association with radiocarbon data.

(2) $Z_{dif} = Z_{DSM} - Z_{grd}$

In this equation, Z_{dif} represents the vertical differences, Z_{DSM} denotes the Z value from the 3D dense point cloud, and Z_{grd} is the Z value from the Antenna Catalyst/theodolite checkpoint. The Z_{dif} values were found to be under 10 cm. Given that the Antenna Catalyst data has an error margin of ± 20 cm, a vertical error tolerance of ± 20 cm was accepted for the 3D models. The final digital terrain model was then refined based on the Z_{dif} values.

3.5. Sediment core

The core SF-08, published by de Azevedo et al. (2021), was integrated with new cores SF-07, SF-09, and SF-10 (Table 1). These cores were collected during the winter season in August 2017 using Russian-type sampling equipment (Fig. 1c and Fig. 3d). The cores were subsampled at 5 cm intervals for grain-size analysis, organic geochemistry, and pollen analysis. Based on the sedimentation rates (Table 2), the chosen sampling interval provides a temporal resolution of 50 to 125 years, which is well-suited to the objectives of this study.

3.6. Facies analysis

The cores were X-rayed to examine internal sedimentary structures. It allowed us to identify continuous and undisturbed sequences. Samples were collected only from laminated intervals, free of evidence of bioturbation or sediment reworking, thereby preserving the original stratigraphic integrity. Grain size analysis was conducted using laser diffraction with a SHIMADZU SALD 2101 laser particle size analyzer in the Laboratory of Chemical Oceanography at Federal University of Pará (UFPA). Approximately 0.5 g of each sample was treated with H_2O_2 to remove organic matter, and the remaining sediments were disaggregated using ultrasound. The grain-size classification included sand (2–0.0625 mm), silt (62.5–3.9 μm), and clay (3.9–0.12 μm) fractions, based on the scale from (Wentworth, 1922). For facies analysis, the methods of (Harper, 1984; Walker, 1992) were applied, which involved describing the color, lithology, texture, and structure. The sedimentary facies were classified according to (Miall, 1978).

3.7. Pollen analysis

The sediment cores were subsampled (1 cm^3) at 5 cm intervals, resulting in a total of 125 samples that were processed using standard pollen analytical techniques, including acetolysis (Faegri and Iversen, 1989). Reference sources for pollen grain and spore identification included morphological descriptions by (Colinvaux P, 1999; Herrera and Urrego, 1996; JE, 1991; Lorente et al., 2017). At least 300 pollen grains were counted from each muddy sample. The software packages TILIA and TILIAGRAPH were utilized to calculate and generate pollen diagrams (Grimm, 1990), while CONISS was employed for cluster analysis of pollen taxa, enabling the zonation of the pollen diagram (Grimm, 1987).

Table 1
Geographic coordinates, total length, elevation, and vegetation type at each sediment core sampling site in the Babitonga Bay region, southern Brazil.

Core	Latitude/ longitude	Length (cm)	Sampling site elevation (cm above mean sea-level)	Vegetation
SF-7	26° 12′ 50.5830″ S, 48° 34′ 27.9289″ W	200	15	Mangrove
SF-8	26° 12′ 52.8916″ S, 48° 34′ 27.7555″ W	200	170	Mangrove
SF-9	26° 12′ 54.5092″ S, 48° 34′ 27.7257″ W	200	190	Herbaceous flat
SF-10	26° 12′ 56.1458″ S, 48° 34′ 26.5479″ W	100	260	Ombrophilous forest

3.8. Organic geochemistry

A total of 125 samples (ranging from 6 to 50 mg) were collected at 5 cm intervals from sediment cores to analyze vegetation changes and explore variations in organic matter sources. The sediments were treated with 4 % hydrochloric acid (HCl) to remove carbonates, then washed with distilled water until the pH reached 6. They were subsequently dried at 50 °C and homogenized. The samples were analyzed for total organic carbon (TOC) and total nitrogen (TN) at the Stable Isotope Laboratory of CENA/USP. Results were expressed as a percentage of dry weight, with analytical precision of 0.09 % for TOC and 0.07 % for TN. The $\delta^{13}C$ values were reported in per mille (‰) relative to VPDB, with a precision of 0.2 ‰. The elemental data were used to calculate the C/N (weight/weight) ratio for all samples. The determination of organic matter sources is environment-dependent, based on $\delta^{13}C$ and C/N composition (Lamb et al., 2006). Despite being potentially affected by post-depositional processes, the C/N ratio remains a widely used and robust proxy for identifying the sources of sedimentary organic matter and reconstructing past environmental conditions, particularly when interpreted alongside stable carbon isotopes ($\delta^{13}C$). While nitrogen can be more susceptible to early diagenetic alteration due to its association with labile proteinaceous compounds, multiple studies have shown that source-specific C/N signatures can still be preserved under favorable conditions (Goñi et al., 1998; Lamb et al., 2006; Meyers, 1994). To ensure the reliability of C/N data in this study, all sediment cores were radiographed prior to sampling. In mangrove and saltmarsh settings, where organic inputs from terrestrial plants and aquatic sources differ significantly in C/N and $\delta^{13}C$ values, this multiproxy approach has proven effective in identifying vegetational shifts linked to relative sea-level changes (Lamb et al., 2006). Therefore, the observed variations in C/N ratios, especially when consistent with $\delta^{13}C$ trends and sedimentological features, are interpreted as reliable indicators of coastal wetland dynamics during the Holocene (Cohen et al., 2021, 2020a; Cohen et al., 2014; França et al., 2014; Francisquini et al., 2014; Ribeiro et al., 2018).

3.9. Radiocarbon dating

The chronology of events was established using 9 radiocarbon dates obtained through accelerator mass spectrometry (AMS). Sedimentary samples were carefully inspected and physically cleaned under a stereomicroscope to prevent natural contamination. The organic material was chemically treated to remove more recent organic substances, such as fulvic and/or humic acids and carbonates. This treatment involved removing remaining material with 2 % HCl at 60 °C for 4 h, followed by cleaning with distilled water to neutralize the pH and drying at 50 °C (Pessenda et al., 2012). All samples were combusted in the benzene synthesis line, transformed to CO_2 and encapsulated at the ^{14}C Laboratory of CENA. Sedimentation rates were estimated using the sample depths and time intervals. The CO_2 samples were analyzed at the AMS Radiocarbon Laboratory (UGAMS), Center for Applied Isotope Studies, University of Georgia, Georgia, USA. Radiocarbon ages were normalized to a $\delta^{13}C$ of − 25 ‰ VPDB and are reported as calibrated years before present (cal yr BP; 2σ), using CALIB 8.2, (Stuiver, 1993), where "present" is defined as 1950 CE. The dates are presented in the text as the median of the calibrated age ranges (Table 2). The RBacon model was applied to the radiocarbon (C14) dates using the SHCal20 calibration curve to develop age-depth relationships for the studied cores (Hogg et al., 2020). This approach, which is based on Bayesian statistical methods, reconstructs sediment accumulation histories and enables the estimation of ages for stratigraphic layers without direct dating (Blaauw

Table 2
Samples of sedimentary organic matter selected for radiocarbon dating. Laboratory number, sample identification with depth (cm), 14C ages (percentage of Modern Carbon, yr BP, 1σ), calibrated ages (cal. yr BP, 2σ deviation), and median of calibrated ages (cal. yr BP).

UGAMS	ID	pMC	±	14C age yr, BP	±	Ages (cal yr BP, 2σ)	Median of age range	Sed. rate (mm/yr)
28,834	SF10 55–60	84.618	0.262	1341	24	1177–1278	1227	0.4
28,835	SF10 89–93	82.134	0.252	1581	24	1364–1517	1419	1.8
28,836	SF09 105–110	79.675	0.23	1825	23	1692–1748	1720	0.6
28,837	SF08 60–65	92.901	0.288	591	24	518–560	546	1.0
28,838	SF08 115–120	84.573	0.245	1345	23	1178–1279	1226	0.7
28,839	SF07 29–34	109.319	0.313			1963 CE	1963 CE	7.5
28,840	SF07 80–85	93.318	0.371	555	23	507–549	530	0.9
28,841	SF07 100–105	92.793	0.271	600	23	525–561	551	1.0
28,842	SF07 170–175	82.009	0.256	1593	25	1398–1521	1443	0.8

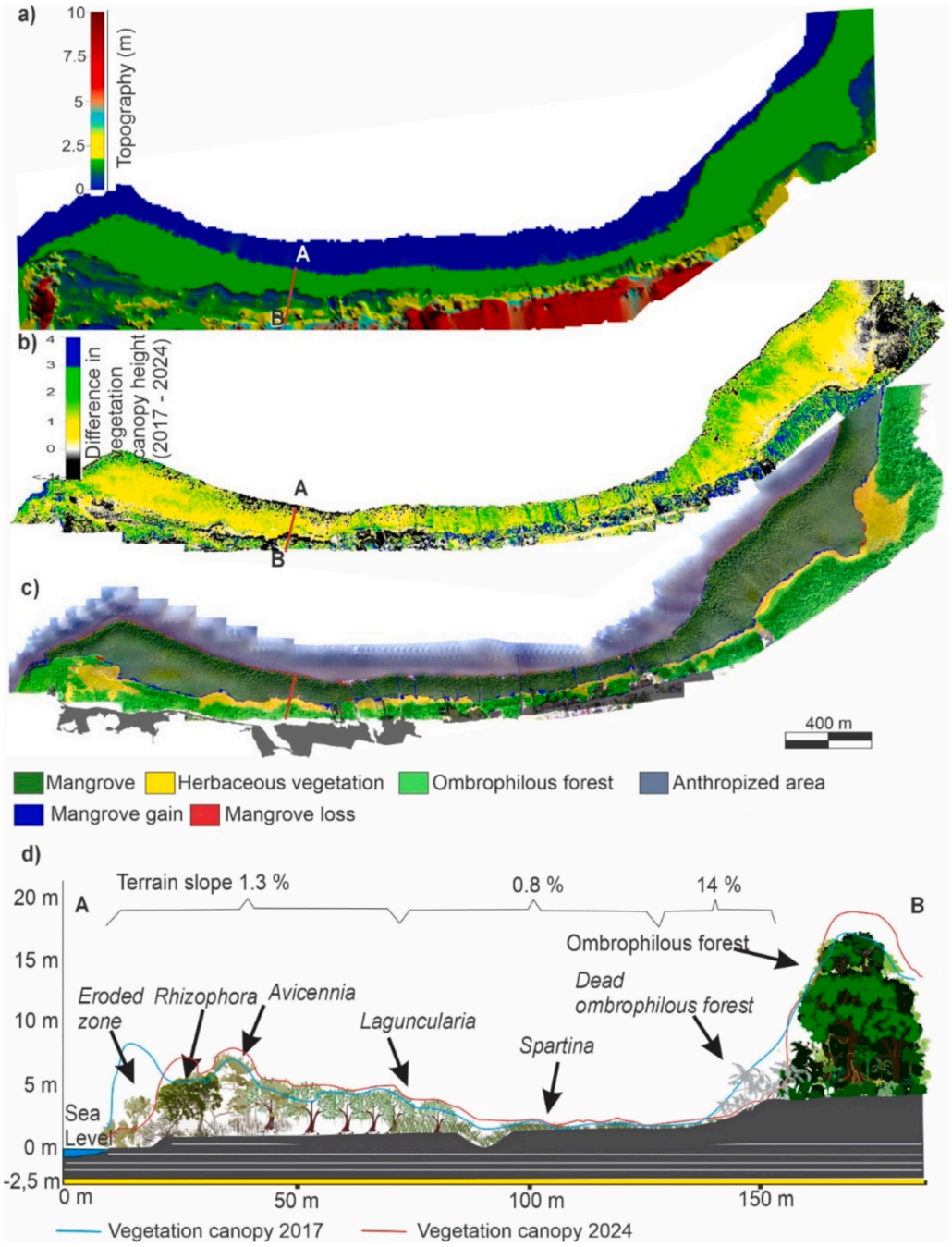

Fig. 4. A) Digital terrain model based on dense point clouds. b) Spatial-temporal analysis evidencing the difference in the vegetation canopy height, and c) the losses and gains in mangrove area between 2017 and 2024. d) Elevation transects indicating the decrease and increase of mangrove canopy height along the lower and higher intertidal flats, respectively.

and Christen, 2011). The nine radiocarbon dates provide a reasonable chronological framework for reconstructing mangrove development stages, and the results are consistent with other studies from the Brazilian coast (e.g. Cohen et al., 2012; Cohen et al., 2020 and Cohen et al., 2021). However, as with any radiocarbon-based chronology, some degree of uncertainty must be considered, particularly due to potential reservoir effects, calibration ranges, and local taphonomic processes (Geyh and Schleicher, 1990; Reimer and Reimer, 2001; Stuiver and Polach, 1977). These uncertainties may slightly affect the precise timing of individual events, but they do not alter the overall trends observed in mangrove expansion and retreat. Although the use of ^{210}Pb dating could, in principle, enhance the chronological resolution of the recent sedimentary record, its applicability is generally limited to the past ~100–150 years due to the relatively short half-life of unsupported ^{210}Pb (~22.3 years). This approach is commonly used in studies addressing modern sedimentation rates. In our study, the most recent mangrove dynamics of interest began around 530 cal yr BP, extending beyond the effective temporal range of ^{210}Pb dating. Additionally, we emphasize that the reliability of our radiocarbon chronology for the last ~150 years is supported by previous comparisons of ^{14}C and ^{210}Pb dating in similar muddy tidal flat settings (Cohen et al., 2020b).

4. Results

4.1. Vegetation and morphology

In the lower areas of the coastal plain (0–2 m above mean sea level, amsl), tidal flats with gentle slopes (0.8–1.3 %) are occupied by mangroves and herbaceous vegetation. Near the shore (0–20 cm amsl, salinity ~30 ‰), *Avicennia* dominates in sparse stands (2–3 m spacing), reaching 6–10 m in height and ~20 cm in diameter at breast height (DBH), with occasional *Laguncularia* and *Rhizophora* (~6 m tall). A denser (~2 m between-tree spacing) *Laguncularia* zone (3–5 m tall, 10–15 cm DBH) occurs between 20–170 cm amsl (salinity ~28 ‰). Higher herbaceous flats (100–200 cm amsl) are dominated by *Spartina* (~0.8 m tall). A steep slope (~14 %) marks the transition to a coastal terrace (>2 m amsl), covered by ombrophilous forest (15–20 m tall, ~30 cm DBH), influenced solely by rainfall.

4.2. Spatial-temporal analysis (2017–2024)

Most mangrove loss (0.8 ha) occurred in the lowest mudflat zone (0–10 cm amsl), marked by shoreline retreat and a reduction in tree height. In contrast, mangroves expanded by 2.3 ha—primarily *Laguncularia*—in the transition to the herbaceous flat (~170 cm amsl), with canopy height increases of 1–3 m in intermediate (100–150 cm amsl) and 0–1 m in higher (150–170 cm amsl) tidal flats. Ombrophilous forest declined near the herbaceous flat (~200 cm amsl) but showed canopy height gains (1–4 m) on the upper coastal terrace (Fig. 4b and d).

4.3. Radiocarbon ages and sedimentation rates

Radiocarbon data revealed ages ranging from 1720 cal yr BP to 1963 CE (Table 2). The estimated sedimentation rates were lower between 1440 and 530 cal yr BP (1.8–0.6 mm/yr) than between 530 cal yr BP – modern ages (7.5–0.9 mm/yr) (Figs. 5–8). These estimates are similar to the rates obtained for tidal flats colonized by mangroves on the Brazilian coast (Cohen et al., 2020a, 2012, 2009, 2008, 2005b, 2005a; Franca et al., 2016; França et al., 2014, 2012; Guimarães et al., 2012, 2010; Lara and Cohen, 2009; Moraes et al., 2017; Smith et al., 2011). Given that all these cores were taken from intertidal flats with mangroves developed according to similar accommodation space (Spencer and Möller, 2013), constancy in these sedimentation rates can be predicted.

4.4. Facies description

Four facies associations were recognized in the analyzed cores based on sedimentary characteristics, pollen, stable isotopes (δ^{13}C), and elemental data (C/N ratio), as outlined below (Table 3).

4.4.1. Facies association A (Estuarine channel)

This facies association, found in cores SF7, SF8, and SF9, dates to before ~1400 cal yr BP and consists of a fining-upward sequence from massive to cross-bedded sand. It is dominated by tree/shrub pollen

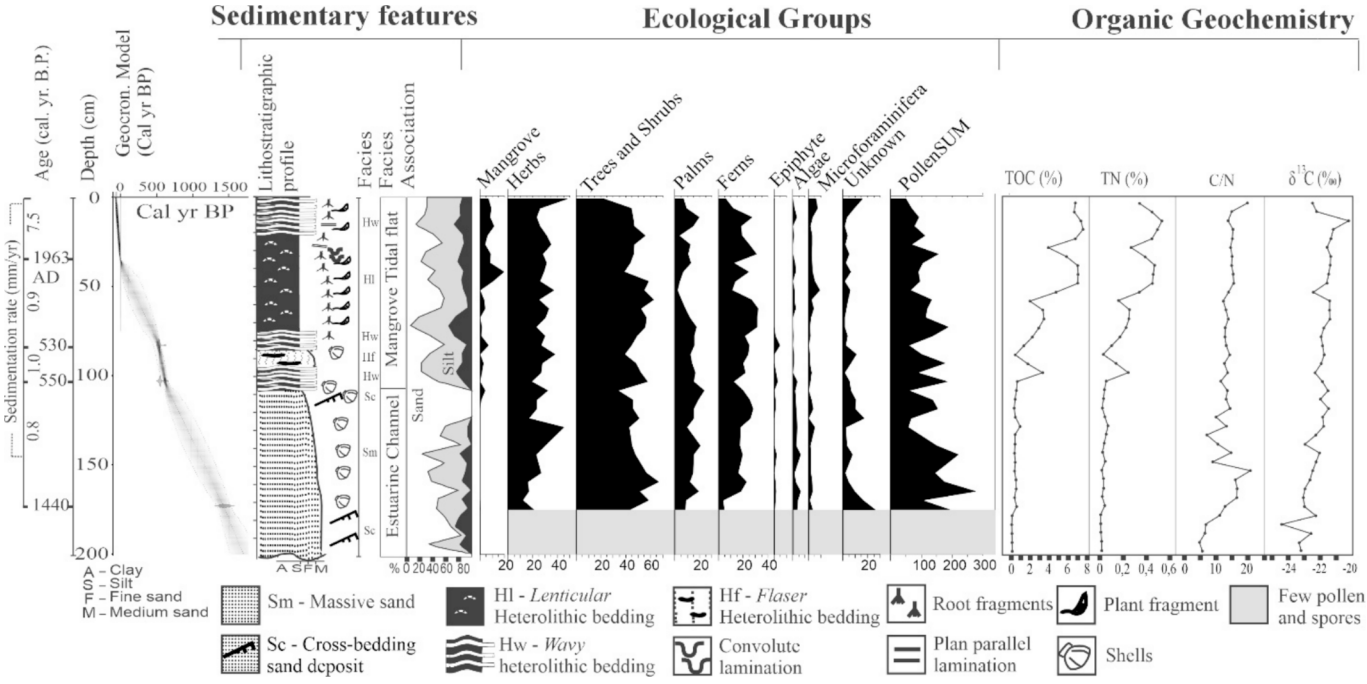

Fig. 5. Summary of core SF-7, presenting geochronological model, sedimentary characteristics, facies association (A – Estuarine channel and B – Mangrove tidal flat), grain size analysis, pollen ecological groups, and geochemical data.

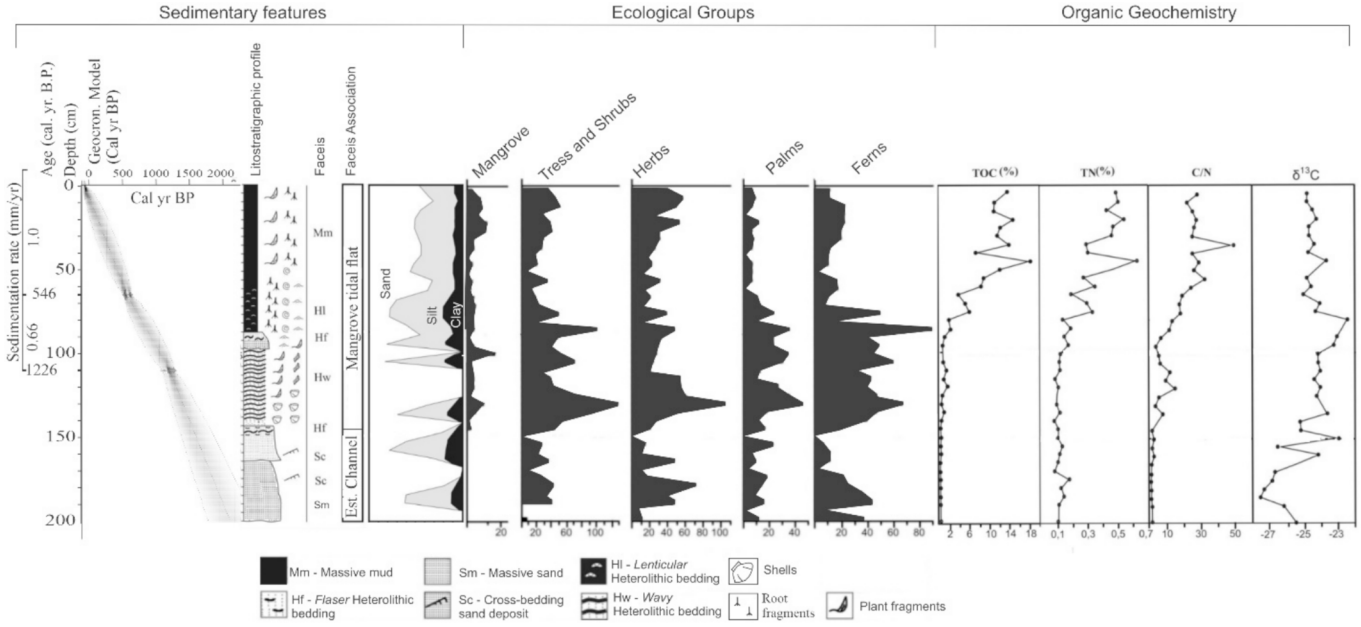

Fig. 6. Summary of core SF-8, presenting geochronological model, sedimentary characteristics, facies association (A – Estuarine channel and B – Mangrove tidal flat), grain size analysis, pollen ecological groups, and geochemical data (data published by Azevedo et al., 2021).

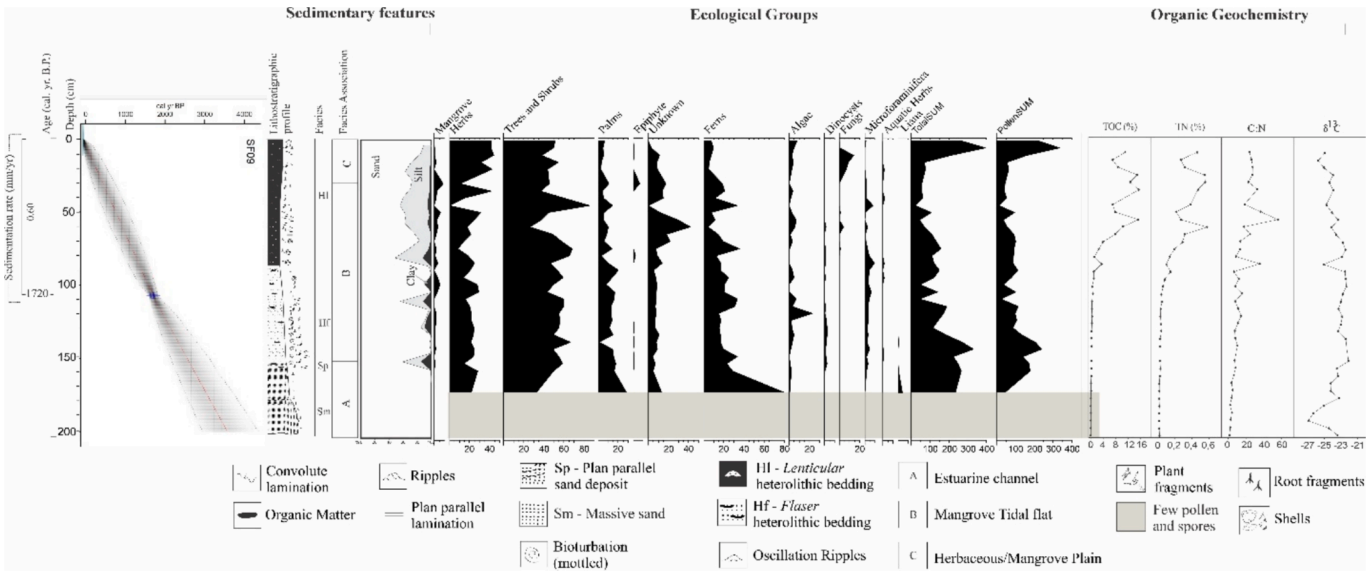

Fig. 7. Summary of core SF-9, presenting geochronological model, sedimentary characteristics, facies association (A – Estuarine channel, B – Mangrove tidal flat and C- Herbaceous tidal flat), grain size analysis, pollen ecological groups, and geochemical data.

(40–70 %) and herbaceous taxa (15–45 %). $\delta^{13}C$ values range from −21.6 ‰ to −24.5 ‰ ($\bar{x}$ = −22 ‰), and C/N ratios from 6 to 20 ($\bar{x}$ = 10) (Figs. 5–8, and Figs. S1, S2 and S3 in Supplementary material).

4.4.2. Facies association B (Mangrove tidal flat)

This facies association was identified in cores SF7, SF8, SF9, and SF10, spanning elevations from 90 cm below mean sea level to 206 cm amsl and ages from > 1700 to 0 cal yr BP. The sediments comprise dark gray massive mud and heterolithic bedding (lenticular, wavy, and flaser), with pollen from mangroves (*Laguncularia*, *Rhizophora*, *Avicennia*), herbs (Poaceae, Asteraceae, Cyperaceae), trees/shrubs (*Alchornea*, Myrtaceae, Myrsinaceae, Fabaceae, *Didymopanax*), palms, ferns, and foraminifera. *Rhizophora* pollen appears only after 1850 CE. $\delta^{13}C$ values decreased from −20 ‰ to −26 ‰ ($\bar{x}$ = −24 ‰), while C/N ratios rose from 8 to 58 ($\bar{x}$ = 13), especially in cores from the higher tidal flats (Figs. 5–8 and Figs. S1-S4).

4.4.3. Facies association C (Herbaceous tidal flat)

Identified in cores SF9 (30–0 cm) and SF10 (54–28 cm), these dark gray lenticular heterolithic deposits accumulated between ~1100 cal yr BP and today, at elevations of 160–232 cm amsl. They are characterized by dominant herb (15–45 %) and tree/shrub (40–55 %) pollen. $\delta^{13}C$ values range from −24 ‰ to −27.5 ‰ ($\bar{x}$ = −25 ‰), with C/N ratios from 12 to 42 ($\bar{x}$ = 28) (Figs. 7 and 8, Table 3).

4.4.4. Facies association d (Ombrophilous forest terrace)

Found only in core SF10 (28–0 cm), these dark gray organic massive mud deposits accumulated between 232 and 260 cm amsl (~500 cal yr

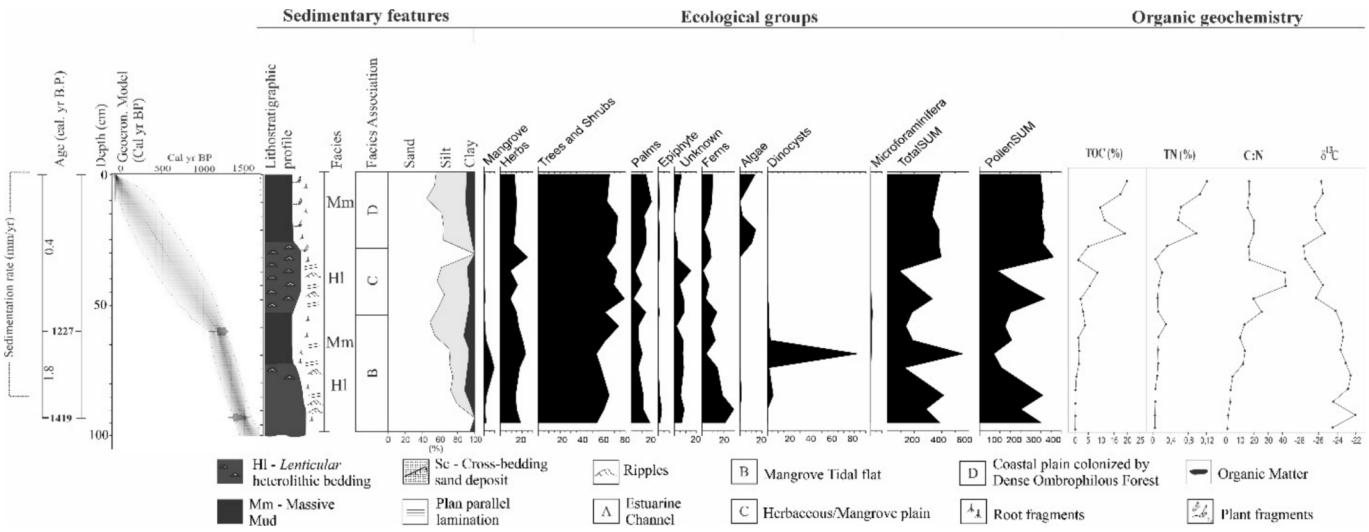

Fig. 8. Summary of core SF-10, presenting geochronological model, sedimentary characteristics, facies association (B – Mangrove tidal flat, C- Herbaceous tidal flat and D- Ombrophilous forest terrace), grain size analysis, pollen ecological groups, and geochemical data.

Table 3
Facies associations proposed for the studied cores according to sedimentary features, pollen, and geochemical data.

Facies association	Facies description	Ecological group	Geochemical data	Interpretation
A	Massive sand (Sm), cross-bedding sand (Sc) and wavy (Hw)/flaser (Hf) heterolithic bedding	Tree/shrubs (20 – 68 %), herbs (15 – 70 %), palms (10 – 25 %), mangrove (0 – 5 %), ferns, and foramenifera	$\delta^{13}C$ = -21.6 – −24.5 ‰ ($\bar{x}$ = − 22 ‰) C/N = 6–20 ($\bar{x}$ = 10)	Estuarine Channel
B	Massive mud (Mm), lenticular (Hl), wavy (Hw) and flaser (Hf) heterolithic bedding	Mangrove (5–20 %), herbs (25 – 45 %), tree/shrubs (25 – 60 %), palms (5 – 20 %), ferns, and foramenifera	$\delta^{13}C$ = -20 – −26 ‰ ($\bar{x}$ = − 24 ‰) C/N = 8–58 ($\bar{x}$ = 13)	Mangrove tidal flat
C	Lenticular heterolithic bedding (Hl)	Herbs (15 – 45 %), tree/shrubs (40 – 55 %), palms (0 – 5 %), mangrove (0 – 1 %), ferns, and foraminifera	$\delta^{13}C$ = -24 – −27.5 ‰ ($\bar{x}$ = − 25 ‰) C/N = 12–42 ($\bar{x}$ = 28)	Herbaceous tidal flat
D	Massive mud (Mm)	Tree/shrubs (65 – 75 %), herbs (10 – 15 %), palms (15 – 20 %), mangrove (0 %) and ferns	$\delta^{13}C$ = -25 – −27.5 ‰ ($\bar{x}$ = − 26.5 ‰) C/N = 16–20 ($\bar{x}$ = 18)	Rainforest coastal plateau

BP to present). Pollen data show dominance of trees/shrubs (65–75 %), with herbs (10–15 %) and palms (15–20 %). $\delta^{13}C$ values range from −25 ‰ to −27.5 ‰ ($\bar{x}$ = −26.5 ‰), and C/N ratios from 16 to 20 ($\bar{x}$ = 18).

5. Discussion

5.1. Seaward mangrove migration due to sea-level fall in the late Holocene

Mid-Holocene sea-level highstand (4–5 m above present) occurred ~5500 cal yr BP (Angulo et al., 2006; Angulo and Lessa, 1997; Boski et al., 2015; Cohen et al., 2021, 2020a; Toniolo et al., 2020) (Fig. 9), resulting in the landward migration of mangroves into embayments, estuaries, and lagoons along the Brazilian coast (Bozi et al., 2021; Castro et al., 2010; Cohen et al., 2020a; França et al., 2015; Lorente et al., 2014). The amplitudes of Holocene relative sea-level changes along the Brazilian coast remain a subject of debate, as mid-Holocene highstands appear to have reached higher elevations in the southeast (~5 m) compared to the northeast (~1 m) and northern (~0.6 m) regions of the country (Boski et al., 2015; Ribeiro et al., 2018; Cohen et al., 2020a, Cohen et al., 2021; de Toniolo et al., 2020). Probably, during the mid-Holocene coastal wetlands moved over part of the elevated terraces where highways, houses, and businesses now occur in the study area (Fig. 11d). It was not possible to find evidence of mangrove or saltmarsh presence in the urbanized zone during the mid-Holocene, as these areas have been heavily anthropized, and any traces of such vegetation—such as pollen grains in muddy sediments—have likely been removed or obliterated by the construction of roads, squares, and buildings. However, pollen analysis obtained from elevated coastal plains in the northeastern and southeastern Brazil, which were not yet urbanized, indicated mangrove establishment on higher terraces (3–4 m) during the mid-Holocene (Bozi et al., 2021; Cohen et al., 2020a; 2020b). Therefore, it is reasonable to suggest that these coastal wetlands shifted to higher elevations in the study area during the mid-Holocene. Our data indicated the establishment of mangroves with *Avicennia* and *Laguncularia* along steep surfaces (2–10 %) on the highest flats (1–2 m amsl) between 1700 and 1400 cal yr BP. Following a RSL fall, coastal wetlands migrated to lower flats (~70 cm below modern mean sea level) ~530 cal yr BP (1420 CE), a mangrove establishment that occurred during the Little Ice Age (LIA, ~1300 to 1850 CE, see section 5.3. Sea-level rise since the end of the Little Ice Age) (Figs. 9 and 11c). This regression led to *Spartina* replacing mangroves on higher surfaces (~200 and 160 cm amsl) at the SF10 (~1100 cal yr BP) and SF9 (~400 cal yr BP) sites (Figs. 7 and 8). Meanwhile, mangroves colonized lower flats, and *Spartina* was replaced by ombrophilous forest on the highest flat at SF10 around 500 cal yr BP (1450 CE) (Figs. 8 and 11c). The $\delta^{13}C$ and C/N values from SF8, SF9, and SF10 indicate a shift from marine to terrestrial organic matter between 1700 and 500 cal yr BP, supporting a marine regression during this period (Fig. 10). Even during the higher sea-level (~1700 cal yr BP), mangroves persisted in the study area (Fig. 11d). The interpretation of RSL trends derived from our sediment cores is consistent with previous reconstructions from the southern Brazilian coast. Notably, vermetid reef data from São Francisco do Sul (Toniolo et al.,

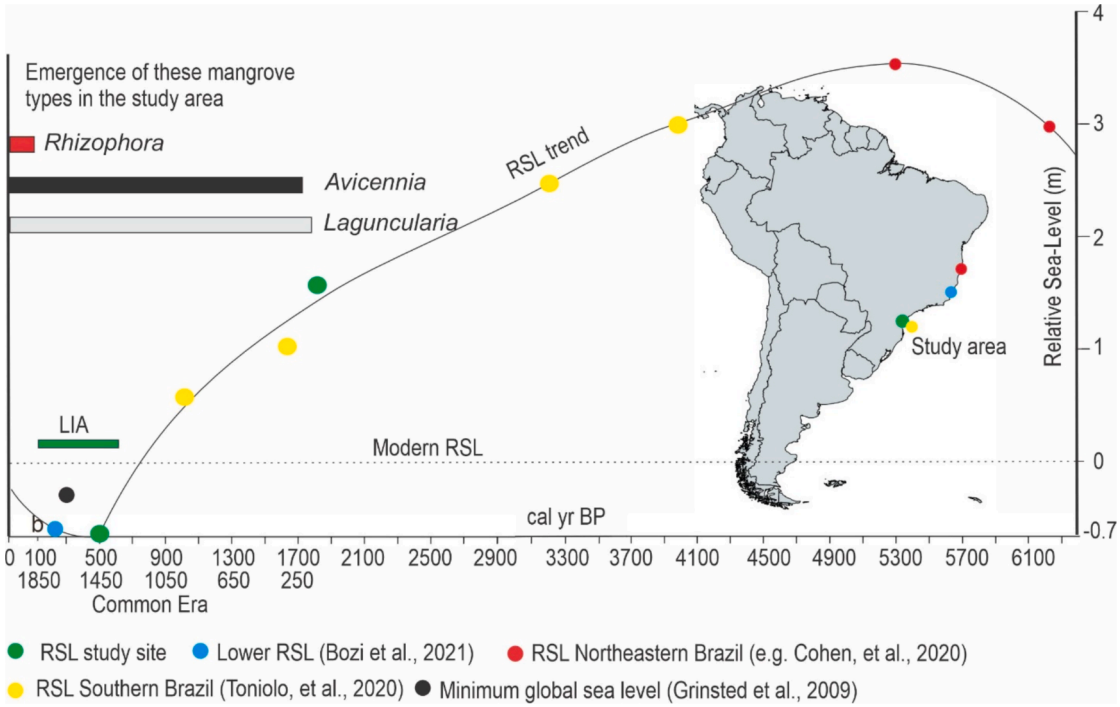

Fig. 9. Timing of the emergence of mangrove types in the study area and the relative sea-level trend from the mid-Holocene to the present along the northeastern and southern Brazilian coast. The figure integrates palaeoecological data with regional sea-level reconstructions to highlight the relationship between mangrove colonization and sea-level dynamics.

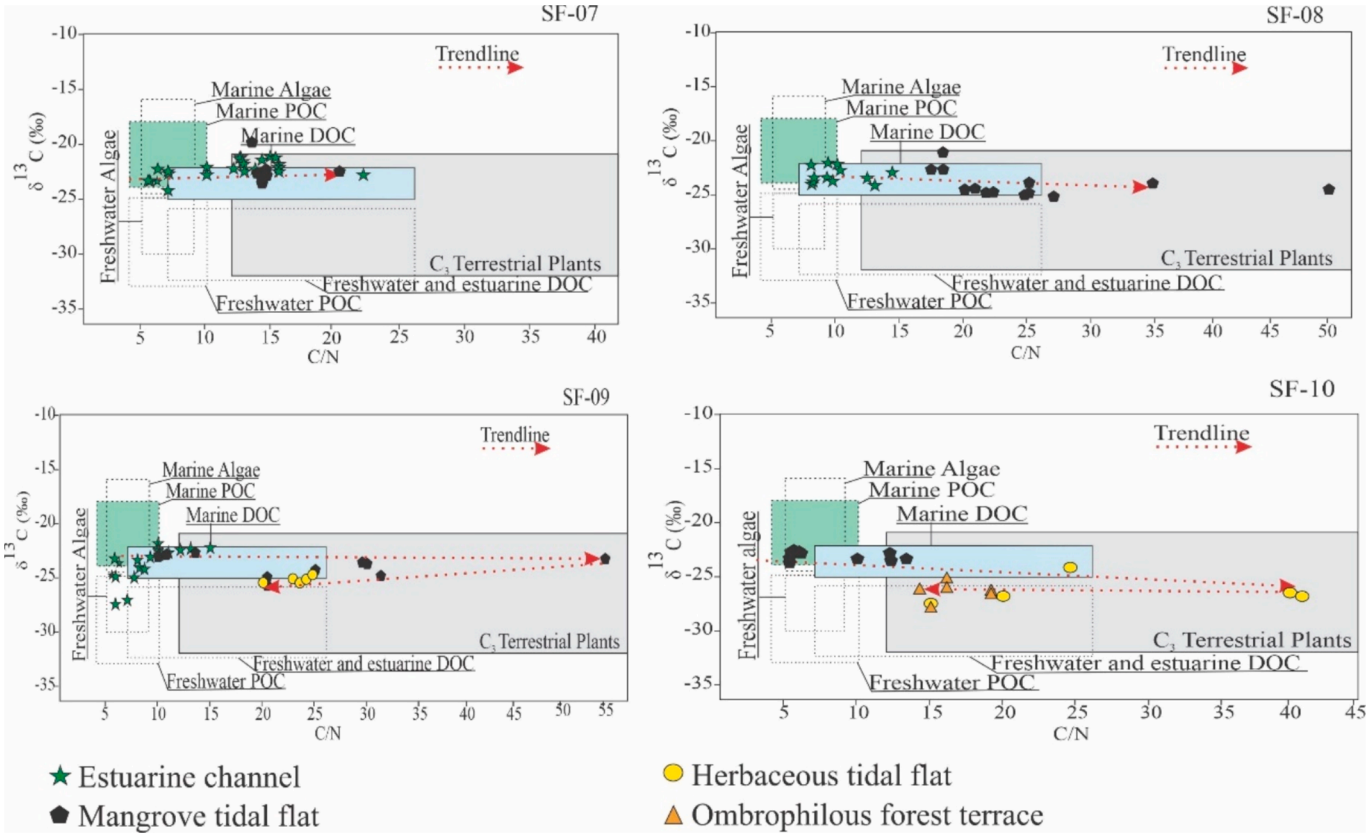

Fig. 10. Binary diagram ($\delta^{13}C$ and C/N) indicating the changes in the source of the sedimentary organic matter for studied cores during the late Holocene.

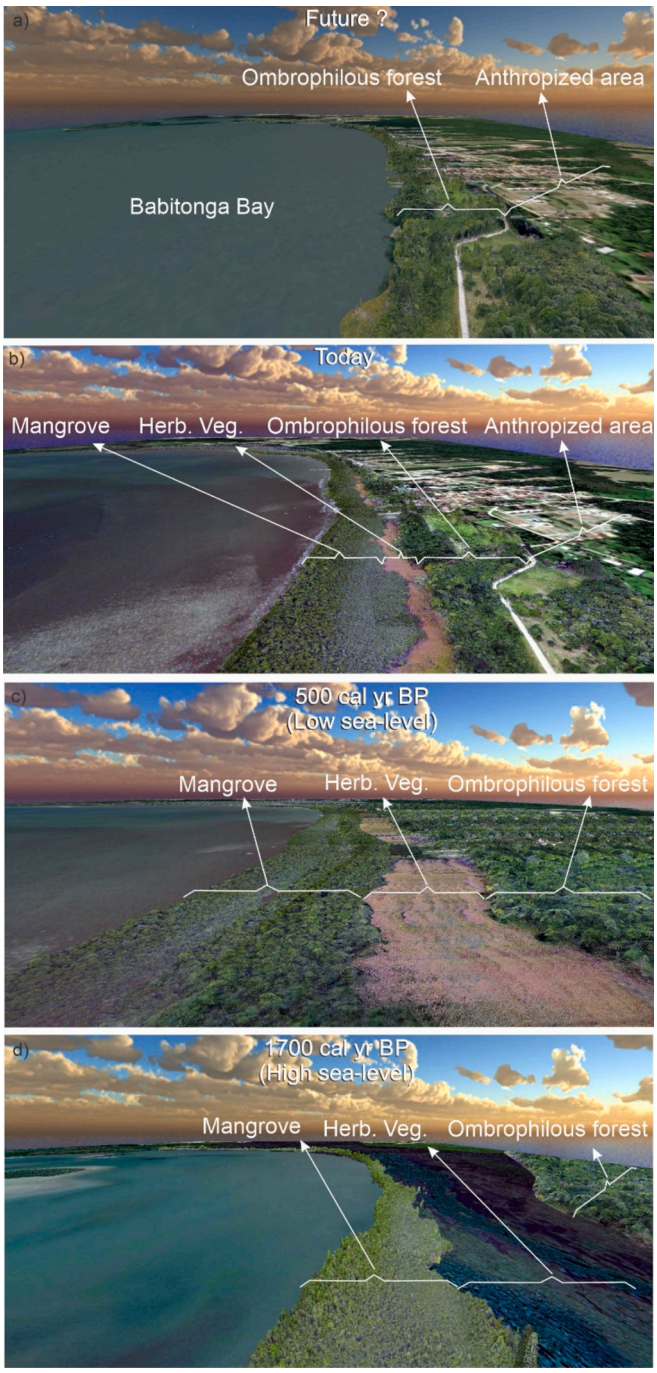

Fig. 11. Model of geomorphology and vegetation development under late Holocene and Anthropocene RSL changes, highlighting: a) the threat of mangrove squeeze due to coastal urbanization associated with RSL rise. b) The modern zonation of coastal vegetation and anthropized areas. c) Seaward expansion; and d) landward migration of coastal vegetation according to fall and rise in RSL, respectively.

2020) indicated a progressive RSL fall during the late Holocene. Their data shows a maximum RSL of + 2.9 m at ~4000 cal yr BP and a gradual decrease to + 0.5 m by ~900 cal yr BP. This long-term regression trend corroborates our findings of mangrove colonization on higher intertidal flats (~1.5 m above present RSL) around ~1700 cal yr BP, followed by their downslope migration (~70 cm below present RSL) by ~530 cal yr BP (Fig. 9). A similar trend was recorded near Guarapari, in the southern part of Espírito Santo State on the northeastern Brazilian coast, where paleoecological studies revealed a seaward mangrove migration between 2700 cal yr BP and 77 cal yr BP (1873 CE) (Bozi et al., 2021). The Jucuruçu River, State of Bahia-Northeastern Brazil, and Macucós Lake, northern State of Espírito Santo, southeastern Brazil, had mangrove forests ~37 km inland within the estuary and ~23 km inland of the modern coastline, respectively, due to the RSL rise during the mid-Holocene. Since then, RSL has fallen, reducing tidal water salinity towards the late Holocene, resulting in mangroves being replaced with freshwater floodplain vegetation (Buso Junior, 2013; Cohen et al., 2020a). According to Angulo et al. (2006), this late-Holocene RSL fall is primarily attributed to glacio-isostatic adjustments (GIA) associated with the viscoelastic response of the Earth's lithosphere and mantle to ice-sheet melting after the Last Glacial Maximum. While local tectonic processes may also influence RSL trends in specific areas, the general pattern of sea-level fall observed along the northeastern, southeastern, and southern Brazilian coasts is consistent with predictions from GIA models.

5.2. Global warming during the last 2000 years

Multi-proxy data indicate estuarine/marine conditions with foraminifera around 1720 cal yr BP (Fig. 10). *Laguncularia* appeared slightly earlier, followed by *Avicennia* (~1700 cal yr BP), suggesting favorable pollen preservation on the muddy tidal flat. *Rhizophora* was established only after 1850 CE (Fig. 9). Pollen distribution in sediments is mainly influenced by wind strength and distance, distinguishing "local" and "regional" sources with gradual overlap (Davis, 2000; Xu et al., 2012; Andersen, 1967; Janssen, 1966; Sugita, 1994; Behling et al., 2001). Insect-pollinated taxa like *Laguncularia* and *Avicennia* are typically underrepresented in pollen records (Ellison, 2008; Yao et al., 2015; Yao and Liu, 2017). In our study area, *Laguncularia* and *Avicennia* pollen comprise up to 20 % and ~5 % of the total, indicating a mature mangrove forest since ~1700 cal yr BP. *Rhizophora* pollen, more widely dispersed due to wind pollination (Behling et al., 2001; Urrego et al., 2009), appears only after 1850 CE, reflecting regional warming post-Little Ice Age (LIA, ~1300 to 1850 CE). Similar mangrove succession patterns with *Laguncularia, Avicennia*, and *Rhizophora* have been documented in subtropical Brazil (França et al., 2019; Rodrigues et al., 2022), linked to late Holocene temperature increases (e.g. Lohmann et al., 2013; Santos et al., 2013). Mangroves rely on muddy substrates for root anchoring (Cohen et al., 2020a; França et al., 2019), but in southern Brazil, coastal drift limits mud deposition, creating sandy flats that hinder mangrove establishment (Alves, 2009; Cohen et al., 2020b; de Souza Pereira et al., 2010). Thus, the mangrove southern limit is shaped more by geomorphology than by winter temperatures (Cohen et al., 2020b; Yao et al., 2022). With future sea-level rise and human land use, suitable habitats may further decline, intensifying the mangrove squeeze.

5.3. Sea-level rise since the end of the little ice age

Grinsted et al. (2009) reported a global sea-level minimum of −19 to −26 cm around 1730 CE, likely linked to the LIA (~1300 to 1850 CE) (Bradley and Jones, 1992) (Fig. 9). This event was recorded on Brazil's northern (Cohen et al., 2005a) and northeastern coasts (Bozi et al., 2021) between 390 and 77 cal yr BP (1560–1873 CE). Since ~77 cal yr BP (1873 CE), mangroves have expanded onto higher tidal flats previously occupied by herbs, palms, and trees/shrubs, driven by rising RSL (Bozi et al., 2021; Cohen et al., 2018). The $\delta^{13}C$ and C/N data from SF9 and SF10 indicate a gradual increase in estuarine input up to the present (Figs. 7, 8 and 10), which may be associated with the RSL rise that has occurred since the end of the LIA (Fig. 9). Recent RSL rise led to erosion and mangrove loss in lower intertidal zones (Fig. 4d), while *Laguncularia* expanded into higher areas formerly occupied by *Spartina*. Dead palms at the *Spartina*–ombrophilous forest boundary reflect salinization due to RSL rise. The upper 40 cm of cores SF7 and SF8 show a marked rise in mangrove pollen, likely linked to RSL rise and/or *Rhizophora* expansion

into subtropical zones driven by warmer winters. Natural warming and RSL rise following the end of the LIA triggered this mangrove dynamic. Although industrial-era warming likely accelerated the process, Anthropocene global warming was not the initial driver of mangrove migration into temperate regions and higher elevations (Rodrigues et al., 2021; Rodrigues et al., 2022).

5.4. Global warming and mangroves during the Anthropocene

Mangrove forests can mitigate relative sea-level (RSL) rise, particularly where fluvial sediment input supports coastal accretion (Cohen et al., 2020a). Their roots reduce wave and current energy, promote sediment trapping, and enhance substrate buildup through both external and internal sediment sources. Taller and denser mangroves are more effective at keeping pace with sea-level rise (Breithaupt et al., 2017; Cohen et al., 2020a; Furukawa et al., 1997; Furukawa and Wolanski, 1996; Lovelock et al., 2015b; Woodroffe et al., 2016). Productivity and species composition also influence sediment accumulation and resilience, as different mangroves vary in tolerance to inundation and sedimentation rates (Ellis et al., 2004; Furukawa and Wolanski, 1996; Kathiresan and Kandasamy, 2003; Matos et al., 2020; McKee et al., 2007; Phillips et al., 2017; Di Nitto et al., 2013a, 2013b; Krauss et al., 2003; Rogers et al., 2005). *Rhizophora*, with prop roots, promotes vertical accretion more effectively than *Avicennia*, which has pneumatophores (Furukawa and Wolanski, 1996; Krauss et al., 2003). Mixed stands of *Avicennia* and *Rhizophora* are more efficient at trapping sediments than monospecific stands (Kathiresan Kandasamy, 2003). In our study area, *Rhizophora* established after 1850 CE (Fig. 9), and canopy height increased by 1–3.5 m between 2017 and 2024. This structural growth, along with the presence of three mangrove genera, enhances the forest's ability to keep pace with RSL rise.

Mangrove trees exhibit remarkable adaptability, enabling them to adjust to environmental fluctuations and develop along a wide structural gradient, ranging from dwarf shrubs to tall forests that reach heights of up to 62 m (Cohen et al., 2018, 2024a, 2024b; Simard et al., 2019). Under favorable environmental conditions, such as optimal salinity, warm winter temperatures, and the absence of major disturbances (e.g., hurricanes or severe freezes), mangrove trees may grow rapidly, with annual height increments ranging from 0.3 to 1.0 m in recently colonized areas (Alongi, 2002). However, the mangrove forest analyzed in this study is mature, and these trees should already have reached their maximum stature under stable local environmental conditions. Then, the rise in mangrove canopy height (14–50 cm/yr) in southern Brazil is likely driven by increasing minimum winter temperatures, which are a key factor controlling mangrove growth (Feher et al., 2017; Gabler et al., 2017). Between 1960 and 2002, minimum temperatures rose by + 0.5 °C per decade annually and + 0.4 °C in winter (Marengo and Camargo, 2008). Since mangroves are sensitive to cold (Chapman, 1976; Giri et al., 2011; Walsh, 1974), projected temperature increases of 3–5 °C by 2080 (Marengo, 2006) suggest continued canopy growth and potential expansion into temperate zones (Cohen et al., 2020b; Yao et al., 2022; Cohen et al., 2024a). Mangroves at Cedar Key, Florida, USA, underwent tropicalization, with an increase in canopy height of ~44–50 cm per year between 2000 and 2020 (Cohen et al., 2024a).

While global warming may promote mangrove expansion and taller canopies, rising sea levels could intensify erosion on lower muddy tidal flats, stressing mangroves in subtropical regions. Mangroves can tolerate sea-level rise up to ~7 mm/yr (McKee et al., 2007; Saintilan et al., 2020), but projections under high-emission scenarios (RCP 8.5) suggest rates of 10–20 mm/yr and by 2100, potentially outpacing their adaptive capacity after 2055–2070 (IPCC, 2013; Sasmito et al., 2015). Mangroves in areas with low sediment supply and minimal tidal range are especially vulnerable (Lovelock et al., 2015a; Spencer et al., 2016). Mangroves in Babitonga Bay, characterized by microtidal conditions (0.8–1.5 m) and low sediment supply (Angulo et al., 2006), are likely sensitive to RSL rise. Although mangroves can adapt by migrating landward to higher flats, such as hypersaline areas, coastal development and armoring often block this natural inland movement (Cohen and Lara, 2003; Lara et al., 2002; Leo et al., 2019). In our study area, lower tidal flats with tall mangroves (~12 m) have experienced erosion, creating forest gaps. While new mangroves are establishing on higher flats along the mangrove–herbaceous transition, this shift does not compensate for biomass loss, as mature, tall trees are replaced by younger, shorter ones. This has significant implications for carbon storage: even if mangrove area remains stable, biomass carbon declines, and exposed soils may shift from carbon sinks to sources. The long-term carbon sink function of these mangroves depends on the interplay between RSL rise and coastal topography. Gentle slopes may support continued mangrove migration, while steep gradients could prevent landward expansion and lead to forest loss or collapse (Fig. 11a; Leo et al., 2019). Mangroves in microtidal systems—like our site—are more likely to migrate inland with sea-level rise due to their shallow slopes, but limited sediment supply and low vertical accretion capacity constrain their ability to maintain elevation within the tidal frame (Ellison, 2015; Xie et al., 2022).

Coastal slope and tidal range play key roles in mangrove vulnerability to sea-level rise. Our data indicated a significant increase in the topographic gradient from the coastal plain (slope: 1.3–0.8 %) with mangroves and *Spartina* to the elevated terraces (14 %) dominated by ombrophilous forest, revealing that landward mangrove migration due to the RSL rise should be halted on steeper surfaces. Currently, mangroves reach up to ~170 cm above mean sea level, but beyond ~250 cm, the slope steepens, limiting further expansion. This allows for only ~80 m of potential landward migration before "mangrove squeeze" occurs. With projected sea-level rise rates of 5–10 mm/yr (Kopp et al., 2014), mangrove retreat into this zone may be exhausted between 2105 and 2158 CE. Terraces above 3 m amsl and urban development will further restrict migration, confining mangroves to low-lying areas. Although natural or artificial barriers may shift due to erosion, urban infrastructure is likely to remain, reinforcing these limits. Future mangrove refuges may be floodplains along rivers currently occupied by freshwater vegetation. However, upstream migration will depend on interactions between fluvial discharge and RSL rise, which control saltwater intrusion along river valleys (Bozi et al., 2021; Cohen et al., 2020a).

The elevated terraces that once served as coastal wetlands refuges during the mid-Holocene highstand (Fig. 11d) are now fully urbanized, making future mangrove establishment there unfeasible (Fig. 11b). Thus, assessments of RSL rise impacts must account for both topography and coastal urbanization. Since this terrace–tidal flat configuration is common across southern Brazil, the findings are broadly applicable to the region's subtropical mangroves. While global warming may favor poleward mangrove expansion, it will be constrained by limited horizontal space for landward migration, with natural and urban barriers causing widespread mangrove squeeze (Fig. 11a).

6. Conclusion

Multi-proxy analysis from four sediment cores recorded the effects of the late Holocene RSL changes on the mangroves of Babitonga Bay, southern Brazil. The RSL fall caused a mangrove migration from elevated terraces to the lowest tidal flats, followed by a landward mangrove migration since the end of the LIA, with *Rhizophora* establishment after 1850 CE due to RSL rise and an increase in winter temperatures, respectively. Considering the decade time scale, the loss of mangrove area is the dominant process along the lowest tidal flats, due to rising RSL. However, this forest has migrated to higher flats, and its canopy heights have increased (1–3.5 m) due to a RSL rise and winter temperatures, respectively. The microtidal range, terrain slope, and coastal urbanization will significantly limit landward mangrove migration. Considering the RSL rise rate between 10 and 5 mm/year until 2100, the studied mangroves are likely to shrink considerably between 80 (2105 CE) and 160 years (2158 CE). The pristine elevated terraces

occupied by coastal wetlands during the mid-Holocene high sea-level stand are now urbanized, making it unfeasible to establish mangroves on these surfaces in the face of a RSL rise. Therefore, mangrove expansion to more temperate latitudes in southern Brazil due to global warming will be limited by the relationship between the rate of RSL rise and horizontal space accommodation for landward mangrove migration, where natural and artificial barriers with urbanized zones are highly likely to lead to a mangrove squeeze.

CRediT authorship contribution statement

Marcelo C.L. Cohen: Writing – review & editing, Writing – original draft, Visualization, Validation, Supervision, Software, Resources, Project administration, Methodology, Investigation, Funding acquisition, Formal analysis, Data curation, Conceptualization. **Neuza A. Fontes:** Writing – review & editing, Validation, Formal analysis, Data curation. **Erika Rodrigues:** Writing – review & editing, Validation, Investigation, Formal analysis, Data curation. **Luiz C.R. Pessenda:** Writing – review & editing, Visualization, Validation, Supervision, Resources, Project administration, Methodology, Investigation, Funding acquisition, Formal analysis, Data curation, Conceptualization. **Marlon Carlos França:** Writing – review & editing, Validation, Supervision, Investigation, Formal analysis, Data curation. **Ed Garrett:** Writing – review & editing, Resources, Project administration, Investigation, Funding acquisition. **Junghyung Ryu:** Writing – review & editing, Resources, Project administration, Investigation, Funding acquisition.

Declaration of competing interest

The authors declare that they have no known competing financial interests or personal relationships that could have appeared to influence the work reported in this paper.

Acknowledgments

This study is funded by the Brazilian National Council for Technology and Science (CNPq 304989/2022-3, 403239/2021-4), Research Funding Agency of the State of São Paulo (FAPESP 2020/13715-1), National Research Foundation of Korea (No. RS-2023-00301702), and UK Research and Innovation [NE/Y003187/1]

Appendix A. Supplementary data

Supplementary data to this article can be found online at https://doi.org/10.1016/j.catena.2025.109450.

Data availability

1. Topographic, vegetation, radiocarbon and stratigraphic data (Original data) (PANGAEA)
2. Datasets produced in this article are stored at the PANGAEA Database (https://issues.pangaea.de/browse/PDI-41471) upon publication and accessible to the public for free

References

AgisoftPhotoScan, 2024. AgiSoft Metashape user Manual. Professional Edition Version 2.1. Agisoft LLC. St. Petersburg, Russia. Retrieved from https://www.agisoft.com/downloads/user-manuals/.

Alongi, D.M., 2002. Present state and future of the world's mangrove forests. Environ. Conserv. 29 (3), 331–349. https://doi.org/10.1017/S0376892902000231.

Alvares, C.A., Stape, J.L., Sentelhas, P.C., De Moraes Gonçalves, J.L., Sparovek, G., 2013. Köppen's climate classification map for Brazil. Meteorol. Z. 22, 711–728. https://doi.org/10.1127/0941-2948/2013/0507.

Alves, A.R., 2009. Long-term erosional hot spots in the southern Brazilian coast. J. Geophys. Res. Oceans 114, 2020. https://doi.org/10.1029/2008JC004933.

Andersen, S.T., 1967. Tree-pollen rain in a mixed deciduous forest in south Jutland (Denmark). Rev. Paleobotany and Palynology 3, 267–275.

Angulo, R., Lessa, G., Souza, M., 2006. A critical review of mid- to late-Holocene sea-level fluctuations on the eastern Brazilian coastline. Quat. Sci. Rev. 25, 486–506. https://doi.org/10.1016/j.quascirev.2005.03.008.

Angulo, R.J., Giannini, P.C.F., Suguio, K., Pessenda, L.C.R., 1999. Relative sea-level changes in the last 5500 years in southern Brazil (Laguna-Imbituba region, Santa Catarina State) based on vermetid 14C ages. Mar. Geol. 159, 323–339.

Angulo, R.J., Lessa, G.C., 1997. The Brazilian sea-level curves: a critical review with emphasis on the curves from the Paranaguáand Cananéia regions. Mar. Geol. 140, 141–166. https://doi.org/10.1016/S0025-3227(97)00015-7.

de Azevedo, A.Q., Jiménez-Espejo, F.J., França, M.C., García-Alix, A., da Silva, F.A.B., Pessenda, L.C.R., Cohen, M.C.L., Fontes, N.A., Pinheiro, V.C., Macario, K., Melo, J.C. F., de C Piccolo, M., Bendassolli, J.A., 2021. Hydrological influence on the evolution of a subtropical mangrove ecosystem during the late Holocene from Babitonga Bay, Brazil. Palaeogeogr. Palaeoclimatol. Palaeoecol. 574, 110463. https://doi.org/10.1016/J.PALAEO.2021.110463.

Barros, G.V., Martinelli, L.A., Oliveira Novais, T.M., Ometto, J.P.H.B., Zuppi, G.M., 2010. Stable isotopes of bulk organic matter to trace carbon and nitrogen dynamics in an estuarine ecosystem in Babitonga Bay (Santa Catarina, Brazil). Sci. Total Environ. 408, 2226–2232. https://doi.org/10.1016/J.SCITOTENV.2010.01.060.

Behling, H., Cohen, M.C.L., Lara, R.J., 2001. Studies on Holocene mangrove ecosystem dynamics of the Bragança Peninsula in north-eastern Pará, Brazil. Palaeogeogr. Palaeoclimatol. Palaeoecol. 167, 225–242.

Boski, T., Bezerra, F.H.R., de Fátima Pereira, L., Souza, A.M., Maia, R.P., Lima-Filho, F.P., 2015. Sea-level rise since 8.2ka recorded in the sediments of the Potengi–Jundiai Estuary, NE Brasil. Mar. Geol. 365, 1–13. https://doi.org/10.1016/j.margeo.2015.04.003.

Bozi, B.S., Figueiredo, B.L., Rodrigues, E., Cohen, M.C.L., Pessenda, L.C.R., Alves, E.E.N., de Souza, A.V., Bendassolli, J.A., Macario, K., Azevedo, P., Culligan, N., 2021. Impacts of sea-level changes on mangroves from southeastern Brazil during the Holocene and Anthropocene using a multi-proxy approach. Geomorphology 390, 107860. https://doi.org/10.1016/J.GEOMORPH.2021.107860.

Bradley, R.S., Jones, P.D., 1992. When was the "Little Ice Age"?. In: Mikami, T. (Ed.), Proceedings of the International Symposium on the "Little Ice Age" Climate, Department of Geography, Tokyo Metropolitan University. pp. 1–4.

Breithaupt, J.L., Smoak, J.M., Rivera-Monroy, V.H., Castañeda-Moya, E., Moyer, R.P., Simard, M., Sanders, C.J., 2017. Partitioning the relative contributions of organic matter and mineral sediment to accretion rates in carbonate platform mangrove soils. Mar. Geol. 390, 170–180. https://doi.org/10.1016/J.MARGEO.2017.07.002.

Burrows, M.T., Schoeman, D.S., Buckley, L.B., Moore, P., Poloczanska, E.S., Brander, K. M., Brown, C., Bruno, J.F., Duarte, C.M., Halpern, B.S., Holding, J., Kappel, C.V., Kiessling, W., O'Connor, M.I., Pandolfi, J.M., Parmesan, C., Schwing, F.B., Sydeman, W.J., Richardson, A.J., 2011. The pace of shifting climate in marine and terrestrial ecosystems. Science 1979 (334), 652–655. https://doi.org/10.1126/science.1210288.

Buso Junior, A.A., 2013. From an estuary to a freshwater lake: a paleo-estuary evolution in the context of holocene sea-level Fluctuations, Southeastern Brazil. Radiocarbon 55. https://doi.org/10.2458/azu_js_rc.55.16210.

Castro, D.F., Rossetti, D.D.F., Ruiz Pessenda, L.C., 2010. Facies, δ13C, δ15N and C/N analyses in a late Quaternary compound estuarine fill, northern Brazil and relation to sea level. Mar. Geol. 274, 135–150. https://doi.org/10.1016/j.margeo.2010.03.011.

Castro, D.F., Rossetti, D.F., Cohen, M.C.L., Pessenda, L.C.R., Lorente, F.L., 2013. The growth of the Doce River Delta in northeastern Brazil indicated by sedimentary facies and diatoms. Diatom Res. 28, 455–466. https://doi.org/10.1080/0269249X.2013.841100.

Cavanaugh, K.C., Kellner, J.R., Forde, A.J., Gruner, D.S., Parker, J.D., Rodriguez, W., Feller, I.C., 2014. Poleward expansion of mangroves is a threshold response to decreased frequency of extreme cold events. PNAS 111, 723–727. https://doi.org/10.1073/pnas.1315800111.

Chapman, V.J., 1976. Mangrove vegetation. ForestryAn Int. J. Forest Res. https://doi.org/10.1016/0006-3207(78)90025-3.

Cohen, M.C.L., Behling, H., Lara, R.J., 2005a. Amazonian mangrove dynamics during the last millennium: the relative sea-level and the Little Ice Age. Rev. Palaeobot. Palynol. 136, 93–108. https://doi.org/10.1016/j.revpalbo.2005.05.002.

Cohen, M.C.L., Behling, H., Lara, R.J., Smith, C.B., Matos, H.R.S., Vedel, V., 2009. Impact of sea-level and climatic changes on the Amazon coastal wetlands during the late Holocene. Veg. Hist. Archaeobot. 18, 425–439. https://doi.org/10.1007/s00334-008-0208-0.

Cohen, M.C.L., Camargo, P.M.P., Pessenda, L.C.R., Lorente, F.L., Souza, A.V.D., Corrêa, J. A.M., Bendassolli, J., Dietz, M., 2021. Effects of the middle Holocene high sea-level stand and climate on Amazonian mangroves. J. Quat. Sci. jqs 3343. https://doi.org/10.1002/JQS.3343.

Cohen, M.C.L., de Souza, A.V., Liu, K., Yao, Q., 2023. A timely method for post-disaster assessment and coastal landscape survey using drone and satellite imagery. MethodsX 10, 102065. https://doi.org/10.1016/J.MEX.2023.102065.

Cohen, M.C.L., de Souza, A.V., Rossetti, D.F., Pessenda, L.C.R., França, M.C., 2018. Decadal-scale dynamics of an Amazonian mangrove caused by climate and sea level changes: inferences from spatial-temporal analysis and digital elevation models. Earth Surf. Proc. Land. 43, 2876–2888. https://doi.org/10.1002/esp.4440.

Cohen, M.C.L., Figueiredo, B.L., Oliveira, N.N., Fontes, N.A., França, M.C., Pessenda, L.C. R., de Souza, A.V., Macario, K., Giannini, P.C.F., Bendassolli, J.A., Lima, P., 2020a. Impacts of Holocene and modern sea-level changes on estuarine mangroves from northeastern Brazil. Earth Surf. Proc. Land. 45, 375–392. https://doi.org/10.1002/esp.4737.

Cohen, M.C.L., França, M.C., Rossetti, D., Pessenda, L.C.R., Giannini, P.C.F., Lorente, F. L., Junior, A.Á.B., Castro, D., Macario, K., 2014a. Landscape evolution during the late Quaternary at the Doce River mouth, Espírito Santo State, Southeastern Brazil.

Palaeogeogr. Palaeoclimatol. Palaeoecol. 415, 48–58. https://doi.org/10.1016/j.palaeo.2013.12.001.
Cohen, M.C.L., Lara, R.J., 2003. Temporal changes of mangrove vegetation boundaries in Amazonia: Application of GIS and remote sensing techniques AN - prod.academic_MSTAR_19222782; 5788855. Wetl. Ecol. Manag. 11, 223–231.
Cohen, M.C.L., Lara, R.J., Smith, C.B., Angélica, R.S., Dias, B.S., Pequeno, T., 2008. Wetland dynamics of Marajó Island, northern Brazil, during the last 1000 years. Catena (Amst.) 76, 70–77.
Cohen, M.C.L., Pessenda, L.C.R., Behling, H., de Fátima Rossetti, D., França, M.C., Guimarães, J.T.F., Friaes, Y., Smith, C.B., 2012. Holocene palaeoenvironmental history of the Amazonian mangrove belt. Quat. Sci. Rev. 55, 50–58.
Cohen, M.C.L., Rodrigues, E., Rocha, D.O.S., Freitas, J., Fontes, N.A., Pessenda, L.C.R., de Souza, A.V., Gomes, V.L.P., França, M.C., Bonotto, D.M., Bendassolli, J.A., 2020. Southward migration of the austral limit of mangroves in South America. Catena (Amst.) 195, 104775. https://doi.org/10.1016/j.catena.2020.104775.
Cohen, M.C.L., Rossetti, D.F., Pessenda, L.C.R., Friaes, Y.S., Oliveira, P.E., 2014b. Late Pleistocene glacial forest of Humaitá-Western Amazonia. Palaeogeogr. Palaeoclimatol. Palaeoecol. 415, 37–47. https://doi.org/10.1016/j.palaeo.2013.12.025.
Cohen, M.C.L., Souza Filho, P.W.M., Lara, R.J., Behling, H., Angulo, R.J., 2005b. A model of Holocene mangrove development and relative sea-level changes on the Bragança Peninsula (northern Brazil). Wetl. Ecol. Manag. 13, 433–443. https://doi.org/10.1007/s11273-004-0413-2.
Cohen, M.C.L., Yao, Q., de Souza, A.V., Liu, K., Pessenda, L.C.R., 2024a. Hurricanes are limiting the mangrove canopy heights in the Gulf of Mexico. Sci. Total Environ. 927, 172284. https://doi.org/10.1016/J.SCITOTENV.2024.172284.
Cohen, M.C.L., Cardenas Ruiz, D.P., Rodrigues, E., Yao, Q., de Souza, A.V., Liu, K.-B., Pessenda, L.C.R., Aragón-Moreno, A.A., Ryu, J., Nunes, S., 2024b. Florida mangrove dieback on a decadal and centennial timescales. Sci. Total Environ. 956, 177345. https://doi.org/10.1016/j.scitotenv.2024.177345.
Colinvaux, P. A., De Oliveira, P. E., & Moreno, J. E. (1999). Amazon Pollen Manual and Atlas. Dordrecht: Harwood Academic Publishers.
Cronin, T.M., 2012. Rapid sea-level rise. Quat. Sci. Rev. 56, 11–30. https://doi.org/10.1016/J.QUASCIREV.2012.08.021.
Cunha, S.R., Tognella-de-Rosa, M.M.P., Costa, C.S.B., 2005. Structure and Litter Production of Mangrove Forests under Different Tidal Influences in Babitonga Bay, Santa Catarina, Southern Brazil [WWW Document]. J Coast Res. URL https://www.jstor.org/stable/25741769 (accessed 2.18.25).
Dangendorf, S., Marcos, M., Wöppelmann, G., Conrad, C.P., Frederikse, T., Riva, R., 2017. Reassessment of 20th century global mean sea level rise. PNAS 114, 5946–5951. https://doi.org/10.1073/pnas.1616007114.
Davis, M.B., 2000. Palynology after Y2K — Understanding the source area of pollen in sediments. Annu. Rev. Earth Planet. Sci. 28, 1–18.
de Souza Pereira, P., Júlio Calliari, L., do Carmo Barletta, R., 2010. Heterogeneity and homogeneity of Southern Brazilian beaches: a morphodynamic and statistical approach. Cont. Shelf Res. 30, 270–280. https://doi.org/10.1016/J.CSR.2009.11.007.
Di Nitto, D., Erftemeijer, P.L.A., van Beek, J.K.L., Dahdouh-Guebas, F., Higazi, L., Quisthoudt, K., Jayatissa, L.P., Koedam, N., 2013a. Modelling drivers of mangrove propagule dispersal and restoration of abandoned shrimp farms. Biogeosciences 10, 5095–5113. https://doi.org/10.5194/bg-10-5095-2013.
Di Nitto, D., Neukermans, G., Koedam, N., Defever, H., Pattyn, F., Kairo, J.G., Dahdouh-Guebas, F., 2013b. Mangroves facing climate change: landward migration potential in response to projected scenarios of sea level rise. Biogeosci. Discuss. 10, 3523–3558. https://doi.org/10.5194/bgd-10-3523-2013.
Ellis, J., Nicholls, P., Craggs, R., Hofstra, D., Hewitt, J., 2004. Effects of terrigenous sedimentation on mangrove physiology and associated macrobenthic communities. Mar. Ecol. Prog. Ser. 270, 71–82. https://doi.org/10.3354/meps270071.
Ellison, J.C., 2015. Vulnerability assessment of mangroves to climate change and sea-level rise impacts. Wetl. Ecol. Manag. 23, 115–137. https://doi.org/10.1007/s11273-014-9397-8.
Ellison, J.C., 2008. Long-term retrospection on mangrove development using sediment cores and pollen analysis: a review. Aquat. Bot. https://doi.org/10.1016/j.aquabot.2008.02.007.
Faegri, K., Iversen, J., 1989. Textbook of Pollen analyses. John Wiley and Sons, New York.
Feher, L.C., Osland, M.J., Griffith, K.T., Grace, J.B., Howard, R.J., Stagg, C.L., Enwright, N.M., Krauss, K.W., Gabler, C.A., Day, R.H., Rogers, K., 2017. Linear and nonlinear effects of temperature and precipitation on ecosystem properties in tidal saline wetlands. Ecosphere 8, e01956. https://doi.org/10.1002/ECS2.1956.
Fox-Kemper, B., Hewitt, H.T., Xiao, C., Aðalgeirsdóttir, G., Drijfhout, S.S., Edwards, T.L., Golledge, N.R., Hemer, M., Kopp, R.E., Krinner, G., Mix, A., Notz, D., Nowicki, S., Nurhati, I.S., Ruiz, L., Sallée, J.-B., Slangen, A.B.A., Yu, Y., 2021. Ocean, Cryosphere and Sea Level Change. In Climate Change 2021: The Physical Science Basis. Contribution of Working Group I to the Sixth Assessment Report of the Intergovernmental Panel on Climate Change [Masson-Delmotte. Cambridge University Press, Cambridge, United Kingdom and New York, NY, USA, pp. 1211–1362. https://doi.org/10.1017/9781009157896.011.
França, M.C., Alves, I.C.C., Castro, D.F., Cohen, M.C.L., Rossetti, D.F., Pessenda, L.C.R., Lorente, F.L., Fontes, N.A., Junior, A.Á.B., Giannini, P.C.F., Francisquini, M.I., 2015. A multi-proxy evidence for the transition from estuarine mangroves to deltaic freshwater marshes, Southeastern Brazil, due to climatic and sea-level changes during the late Holocene. Catena (Amst.) 128, 155–166. https://doi.org/10.1016/j.catena.2015.02.005.
Franca, M.C., Alves, I.C.C., Cohen, M.C., Rossetti, D.F., Pessenda, L.C., Giannini, P.C., Lorente, F.L., Buso Junior, A.A., Bendassolli, J.A., Macario, K., 2016. Millennial to secular time-scale impacts of climate and sea-level changes on mangroves from the Doce River delta, Southeastern Brazil. Holocene 26, 1733–1749. https://doi.org/10.1177/0959683616645938.
França, M.C., Cohen, M.C.L., Pessenda, L.C.R., Rossetti, D.F., Lorente, F.L., Buso Junior, A.Á., Guimarães, J.T.F., Friaes, Y., Macario, K., 2013. Mangrove vegetation changes on Holocene terraces of the Doce River, southeastern Brazil. Catena (Amst.) 110, 59–69.
França, M.C., Francisquini, M.I., Cohen, M.C.L., Pessenda, L.C.R., 2014. Inter-proxy evidence for the development of the Amazonian mangroves during the Holocene. Veg Hist Archaeobot 23. https://doi.org/10.1007/s00334-013-0420-4.
França, M.C., Francisquini, M.I., Cohen, M.C.L., Pessenda, L.C.R., Rossetti, D.F., Guimarães, J.T.F., Smith, C.B., 2012. The last mangroves of Marajó Island — eastern amazon: impact of climate and/or relative sea-level changes. Rev. Palaeobot. Palynol. 187, 50–65.
França, M.C., Pessenda, L.C.R., Cohen, M.C.L., de Azevedo, A.Q., Fontes, N.A., Silva, F.B., de Melo, J.C.F., Piccolo, M.D.C., Bendassolli, J.A., Macario, K., 2019. Late-Holocene subtropical mangrove dynamics in response to climate change during the last millennium. Holocene 29, 445–456. https://doi.org/10.1177/0959683618816438.
Francisquini, M.I., Lima, C.M., Pessenda, L.C.R., Rossetti, D.F., França, M.C., Cohen, M.C.L., 2014. Relation between carbon isotopes of plants and soils on Marajó Island, a large tropical island: implications for interpretation of modern and past vegetation dynamics in the Amazon region. Palaeogeogr. Palaeoclimatol. Palaeoecol. https://doi.org/10.1016/j.palaeo.2014.03.032.
Furukawa, K., Wolanski, E., 1996. Sedimentation in mangrove forests. Mangrove Salt Marshes 1, 3–10. https://doi.org/10.1023/A:1025973426404.
Furukawa, K., Wolanski, E., Mueller, H., 1997. Currents and sediment transport in mangrove forests. Estuar. Coast. Shelf Sci. 44, 301–310. https://doi.org/10.1006/ecss.1996.0120.
Gabler, C.A., Osland, M.J., Grace, J.B., Stagg, C.L., Day, R.H., Hartley, S.B., Enwright, N. M., From, A.S., McCoy, M.L., McLeod, J.L., 2017. Macroclimatic change expected to transform coastal wetland ecosystems this century. Nature Climate Change 2017 7:2 7, 142–147. Doi: 10.1038/nclimate3203.
Geyh, M. A., & Schleicher, H. (1990). Absolute age determination: Physical and chemical dating methods and their application (R. C. Newcomb, Trans.). Springer-Verlag. Doi: 10.1007/978-3-642-74826-4.
Giri, C., Ochieng, E., Tieszen, L.L., Zhu, Z., Singh, A., Loveland, T., Masek, J., Duke, N., 2011. Status and distribution of mangrove forests of the world using earth observation satellite data. Glob. Ecol. Biogeogr. 20, 154–159. https://doi.org/10.1111/J.1466-8238.2010.00584.X.
Goñi, M.A., Ruttenberg, K.C., Eglinton, T.I., 1998. A reassessment of the sources and importance of land-derived organic matter in surface sediments from the Gulf of Mexico. Geochim. Cosmochim. Acta 62, 3055–3075. https://doi.org/10.1016/S0016-7037(98)00217-8.
Grimm, E., 1990. TILIA and TILIAGRAPH: PC spreadsheet and graphic software for pollen data. INQUA Sub-Commission on Data-Handling Methods Newsletter.
Grimm, E.C., 1987. CONISS: a FORTRAN 77 program for stratigraphically constrained cluster analysis by the method of incremental sum of squares. Comput. Geosci. 13, 13–35.
Grinsted, A., Moore, J.C., Jevrejeva, S., 2009. Reconstructing sea level from paleo and projected temperatures 200 to 2100 ad. Clim. Dyn. 34, 461–472. https://doi.org/10.1007/s00382-008-0507-2.
Guimarães, J.T.F., Cohen, M.C.L., França, M.C., Lara, R.J., Behling, H., 2010. Model of wetland development of the Amapá coast during the late Holocene. An. Acad. Bras. Cienc. 82, 451–465. https://doi.org/10.1590/S0001-37652010000200021.
Guimarães, J.T.F., Cohen, M.C.L., Pessenda, L.C.R., Franca, M.C., Smith, C.B., Nogueira, A.C.R., 2012. Mid- and late-Holocene sedimentary process and palaeovegetation changes near the mouth of the Amazon River. Holocene 22, 359–370. https://doi.org/10.1177/0959683611423693.
Hamlington, B.D., Bellas-Manley, A., Willis, J.K., Fournier, S., Vinogradova, N., Nerem, R.S., Piecuch, C.G., Thompson, P.R., Kopp, R., 2024. The rate of global sea level rise doubled during the past three decades. Commun. Earth Environ. 5, 1–4. https://doi.org/10.1038/S43247-024-01761-5;SUBJMETA=106,2739,694,704,829;KWRD=CLIMATE-CHANGE+IMPACTS, OCEAN+SCIENCES.
Harper Jr., C.W., 1984. Facies models revisited: an examination of quantitative methods. Geosci. Can. 11, 203–207.
Herrera, L.F., Urrego, L.E., 1996. Atlas de polen de plantas útiles y cultivadas de La Amazonia colombiana (Pollen atlas of useful and cultivated plants in the Colombian Amazon region). Estudios En La Amazonia Colombiana 9, 462.
Hogg, A.G., Heaton, T.J., Hua, Q., Palmer, J.G., Turney, C.S.M., Southon, J., Bayliss, A., Blackwell, P.G., Boswijk, G., Bronk Ramsey, C., Pearson, C., Petchey, F., Reimer, P., Reimer, R., Wacker, L., 2020. SHCal20 Southern Hemisphere Calibration, 0-55,000 Years cal BP. Radiocarbon 62, 759–778. https://doi.org/10.1017/RDC.2020.59.
IPCC, 2013. Intergovernmental Panel on Climate Change (IPCC) Climate Change 2013: The Physical Science Basis Cambridge University Press, UK, Summary for Policymakers.
Janssen, C.R., 1966. Recent pollen spectra from the deciduous and coniferous deciduous forests of northeastern Minnesota: a study in pollen dispersal. Ecology 47, 804–825.
JE, R.D. and M., 1991. Pollen and Spores of Barro Colorado Island. St. Louis, MO: Missouri Botanical Garden.
Kangas, P.C., Lugo, A.E., Lugo, A.E., 1961. The distribution of mangroves and saltmarsh in Florida. Trop. Ecol. 31, 32–39.
Kathiresan, K., Kandasamy, M., 2003. How do mangrove forests induce sedimentation? Rev. Biol. Trop. 51 (2), 355–359.
Kopp, R.E., Horton, R.M., Little, C.M., Mitrovica, J.X., Oppenheimer, M., Rasmussen, D. J., Strauss, B.H., Tebaldi, C., 2014. Probabilistic 21st and 22nd century sea-level

projections at a global network of tide-gauge sites. Earths Future 2, 383–406. https://doi.org/10.1002/2014EF000239.
Krauss, K.W., Allen, J.A., Cahoon, D.R., 2003. Differential rates of vertical accretion and elevation change among aerial root types in Micronesian mangrove forests. Estuar. Coast. Shelf Sci. 56, 251–259. https://doi.org/10.1016/S0272-7714(02)00184-1.
Lamb, A.L., Wilson, G.P., Leng, M.J., 2006. A review of coastal palaeoclimate and relative sea-level reconstructions using δ13C and C/N ratios in organic material. Earth Sci. Rev. 75, 29–57. https://doi.org/10.1016/j.earscirev.2005.10.003.
Lara, R., Szlafsztein, C., Cohen, M., Berger, U., Glaser, M., 2002. Implications of mangrove dynamics for private land use in Bragança, North Brazil: a case study. J. Coast. Conserv. 8, 97. https://doi.org/10.1652/1400-0350(2002)008[0097:IOMDFP]2.0.CO;2.
Lara, R.J., Cohen, M.C.L., 2009. Palaeolimnological studies and ancient maps confirm secular climate fluctuations in Amazonia. Clim. Change 94, 399–408. https://doi.org/10.1007/s10584-008-9507-9.
Lean, J., Rind, D., 1999. Evaluating sun-climate relationships since the Little Ice Ag. J. Amospheric and Solar-Terrestrial Phys. 61, 25–36.
Leo, K.L., Gillies, C.L., Fitzsimons, J.A., Hale, L.Z., Beck, M.W., 2019. Coastal habitat squeeze: a review of adaptation solutions for saltmarsh, mangrove and beach habitats. Ocean Coast. Manag. 175, 180–190. https://doi.org/10.1016/J.OCECOAMAN.2019.03.019.
Lessa, G.C., Angulo, R.J., Giannini, P.C., Arau, A.D., 2000. Stratigraphy and Holocene evolution of a regressive barrier in south. Brazil 165, 87–108.
Lohmann, G., Pfeiffer, M., Laepple, T., Leduc, G., Kim, J.H., 2013. A model-data comparison of the Holocene global sea surface temperature evolution. Clim. Past 9, 1807–1839. https://doi.org/10.5194/cp-9-1807-2013.
Lorente, F.L., Jr., B., Oliveira, P.E., Pessenda, L.C.R., 2017. Atlas Palinológico: Laboratório 14C – CENA/USP. FEALQ, Piracicaba.
Lorente, F.L., Pessenda, L.C.R., Oboh-Ikuenobe, F., Buso, A.A., Cohen, M.C.L., Meyer, K. E.B., Giannini, P.C.F., de Oliveira, P.E., de F Rossetti, D., Borotti Filho, M.A., França, M.C., de Castro, D.F., Bendassolli, J.A., Macario, K., 2014. Palynofacies and stable C and N isotopes of Holocene sediments from Lake Macuco (Linhares, Espírito Santo, southeastern Brazil): Depositional settings and palaeoenvironmental evolution. Palaeogeogr. Palaeoclimatol. Palaeoecol. 415, 69–82. https://doi.org/10.1016/j.palaeo.2013.12.004.
Lovelock, C.E., Adame, M.F., Bennion, V., Hayes, M., Reef, R., Santini, N., Cahoon, D.R., 2015a. Sea level and turbidity controls on mangrove soil surface elevation change. Estuar. Coast. Shelf Sci. 153, 1–9. https://doi.org/10.1016/j.ecss.2014.11.026.
Lovelock, C.E., Cahoon, D.R., Friess, D.A., Guntenspergen, G.R., Krauss, K.W., Reef, R., Rogers, K., Saunders, M.L., Sidik, F., Swales, A., Saintilan, N., Thuyen, L.X., Triet, T., 2015b. The vulnerability of Indo-Pacific mangrove forests to sea-level rise. Nature 526, 559–563. https://doi.org/10.1038/nature15538.
Blaauw, M., Christen, J.A., 2011. Flexible paleoclimate age-depth models using an autoregressive gamma process. Bayesian Anal. 6, 457–474.
Marengo, J.A., 2006. Mudanças climáticas globais e seus efeitos sobre a biodiversidade: caracterização do clima atual e definição das alterações climáticas para o território brasileiro ao longo do século XXI. Ministério do Meio Ambiente, Brasilia.
Marengo, J.A., Camargo, C.C., 2008. Surface air temperature trends in Southern Brazil for 1960–2002. Int. J. Climatol. 28, 893–904. https://doi.org/10.1002/joc.1584.
Matos, C.R.L., Berrêdo, J.F., Machado, W., Sanders, C.J., Metzger, E., Cohen, M.C.L., 2020. Carbon and nutrient accumulation in tropical mangrove creeks. Amazon Region. Mar. Geol. 429. https://doi.org/10.1016/j.margeo.2020.106317.
Mazzer, A.M., Gonçalves, M.L., 2011. Aspectos geomorfológicos da baía da babitonga, santa catarina , brasil: caracterização morfométric. Revista Brasileira De Geomorfologia 12, 3. https://doi.org/10.20502/RBG.V12I0.264.
McKee, K.L., Cahoon, D.R., Feller, I.C., 2007. Caribbean mangroves adjust to rising sea level through biotic controls on change in soil elevation. Glob. Ecol. Biogeogr. 16, 545–556. https://doi.org/10.1111/j.1466-8238.2007.00317.x.
Meyers, P.A., 1994. Preservation of elemental and isotopic source identification of sedimentary organic matter. Chem. Geol. 114, 289–302. https://doi.org/10.1016/0009-2541(94)90059-0.
Miall, A.D., 1978. Lithofacies types and vertical profile models in braided river deposits: a summary. Fluvial Sedimentology 5, 597–600.
Moraes, C.A., Fontes, N.A., Cohen, M.C.L., Fran?a, M.C., Pessenda, L.C.R., Rossetti, D.F., Francisquini, M.I., Bendassolli, J.A., Macario, K., 2017. Late Holocene mangrove dynamics dominated by autogenic processes. Earth Surf. Proc. Land. https://doi.org/10.1002/esp.4167.
Nobre, C.A., Cavalcanti, P.N., Kayano, M.T., Rao, V.B., Bonatti, J.P., Satyamurti, P., Uvo, C.B., Cohen, J.C., 1986. Aspectos da climatologia dinâmica do Brasil. Climanálise.
Osland, M.J., Day, R.H., Hall, C.T., Brumfield, M.D., Dugas, J.L., Jones, W.R., 2017. Mangrove expansion and contraction at a poleward range limit: climate extremes and land-ocean temperature gradients. Ecology 98, 125–137. https://doi.org/10.1002/ecy.1625.
Osland, M.J., Feher, L.C., 2020. Winter climate change and the poleward range expansion of a tropical invasive tree (Brazilian pepper—Schinus terebinthifolius). Glob. Chang. Biol. 26, 607–615. https://doi.org/10.1111/gcb.14842.
Osland, M.J., Feher, L.C., López-Portillo, J., Day, R.H., Suman, D.O., Guzmán Menéndez, J.M., Rivera-Monroy, V.H., 2018. Mangrove forests in a rapidly changing world: global change impacts and conservation opportunities along the Gulf of Mexico coast. Estuar. Coast. Shelf Sci. 214, 120–140. https://doi.org/10.1016/j.ecss.2018.09.006.
Osland, M.J., Stevens, P.W., Lamont, M.M., Brusca, R.C., Hart, K.M., Waddle, J.H., Langtimm, C.A., Williams, C.M., Keim, B.D., Terando, A.J., Reyier, E.A., Marshall, K. E., Loik, M.E., Boucek, R.E., Lewis, A.B., Seminoff, J.A., 2021. Tropicalization of temperate ecosystems in North America: the northward range expansion of tropical organisms in response to warming winter temperatures. Glob. Chang. Biol. 27, 3009–3034. https://doi.org/10.1111/GCB.15563.
Perry, C.L., Mendelssohn, I.A., 2009. Ecosystem effects of expanding populations of Avicennia germinans in a Louisiana salt marsh. Wetlands 29, 396–406. https://doi.org/10.1672/08-100.1.
Pessenda, L.C.R., Vidotto, E., De Oliveira, P.E., Buso, A.A., Cohen, M.C.L., de F Rossetti, D., Ricardi-Branco, F., Bendassolli, J.A., 2012. Late Quaternary vegetation and coastal environmental changes at Ilha do Cardoso mangrove, southeastern Brazil. Palaeogeogr. Palaeoclimatol. Palaeoecol. 363, 57–68.
Phillips, D.H., Kumara, M.P., Jayatissa, L.P., Krauss, K.W., Huxham, M., 2017. Impacts of Mangrove Density on Surface Sediment Accretion, Belowground Biomass and Biogeochemistry in Puttalam Lagoon, Sri Lanka. Wetlands 37, 471–483. https://doi.org/10.1007/s13157-017-0883-7.
Pinto, M.W., Klein, A.H.F., Almeida, L.P., 2019. BABITONGA BAY MANGROVES: IS THERE A COASTAL SQUEEZE? 1538–1549. Doi: 10.1142/9789811204487_0133.
PIX4D, 2013. Pix4dmapper Software Manual Pix4D Support [WWW Document]. Lausanne, Suiça. Pix4D SA.
Reimer, P.J., Reimer, R.W., 2001. A marine reservoir correction database and on-line interface. Radiocarbon 43 (2A), 461–463. https://doi.org/10.1017/S0033822200038339.
Ribeiro, S.R., Batista, E.J.L., Cohen, M.C., França, M.C., Pessenda, L.C., Fontes, N.A., Alves, I.C., Bendassolli, J.A., 2018. Allogenic and autogenic effects on mangrove dynamics from the Ceará Mirim River, north-eastern Brazil, during the middle and late Holocene. Earth Surf. Proc. Land. https://doi.org/10.1002/esp.4342.
Rodrigues, E., Cohen, M.C.L., Liu, K., Pessenda, L.C.R., Yao, Q., Ryu, J., Rossetti, D., de Souza, A., Dietz, M., 2021. The effect of global warming on the establishment of mangroves in coastal Louisiana during the Holocene. Geomorphology, 107648. https://doi.org/10.1016/j.geomorph.2021.107648.
Rodrigues, R., Cohen, M.C.L., Pessenda, L., França, M., Magalhães, E., Yao, Q., 2022. Poleward mangrove expansion in South America coincides with MCA and CWP: a diatom, pollen, and organic geochemistry studyour Article. Quaternary Sci. Rev. 1.
Rogers, K., Saintilan, N., Cahoon, D., 2005. Surface elevation dynamics in a regenerating mangrove forest at homebush bay, Australia. Wetl. Ecol. Manag. 13, 587–598. https://doi.org/10.1007/s11273-004-0003-3.
Santos, T.P., Franco, D.R., Barbosa, C.F., Belem, A.L., Dokken, T., Albuquerque, A.L.S., 2013. Millennial- to centennial-scale changes in sea surface temperature in the tropical South Atlantic throughout the Holocene. Palaeogeogr. Palaeoclimatol. Palaeoecol. 392, 1–8. https://doi.org/10.1016/j.palaeo.2013.08.019.
Saintilan, N., Khan, N.S., Ashe, E., Kelleway, J.J., Rogers, K., Woodroffe, C.D., Horton, B. P., 2020. Thresholds of mangrove survival under rapid sea level rise. Science 368, 1118–1121. https://doi.org/10.1126/science.aba2656.
Saintilan, N., Wilson, N.C., Rogers, K., Rajkaran, A., Krauss, K.W., 2014. Mangrove expansion and salt marsh decline at mangrove poleward limits. Glob. Chang. Biol. 20, 147–157. https://doi.org/10.1111/gcb.12341.
Salles, F.J.P., 2000. Catálogo de estações maregráficas brasileiras.
Sasmito, S.D., Murdiyarso, D., Friess, D.A., Kurnianto, S., 2015. Can mangroves keep pace with contemporary sea level rise? A global data review. Wetl Ecol. Manag. https://doi.org/10.1007/s11273-015-9466-7.
Schaeffer-Novelli, Y., Cintrón-Molero, G., Soares, M.L.G., De-Rosa, T., 2000. Brazilian Mangroves. Aquat. Ecosyst. Health Manag. 3, 561–570. https://doi.org/10.1080/14634980008650693.
Seluchi, M.E., Marengo, J.A., 2000. Tropical-midlatitude exchange of air masses during summer and winter in South America: climatic aspects and examples of intense events. Int. J. Climatol. 20, 1167–1190.
Simard, M., Fatoyinbo, L., Smetanka, C., Rivera-Monroy, V.H., Castañeda-Moya, E., Thomas, N., Van der Stocken, T., 2019. Mangrove canopy height globally related to precipitation, temperature and cyclone frequency. Nat. Geosci. 12, 40–45. https://doi.org/10.1038/S41561-018-0279-1.
Smith, C.B., Cohen, M.C.L., Pessenda, L.C.R., França, M.C., Guimarães, J.T.F., de F Rossetti, D., Lara, R.J., 2011. Holocene coastal vegetation changes at the mouth of the Amazon River. Rev. Palaeobot. Palynol. 168, 21–30.
Spencer, T., Möller, I., 2013. Mangrove systems. Treatise on Geomorphology 10, 360–391. https://doi.org/10.1016/B978-0-12-374739-6.00290-6.
Spencer, T., Schuerch, M., Nicholls, R.J., Hinkel, J., Lincke, D., Vafeidis, A.T., Reef, R., McFadden, L., Brown, S., 2016. Global coastal wetland change under sea-level rise and related stresses: the DIVA Wetland Change Model. Glob Planet Change 139, 15–30. https://doi.org/10.1016/j.gloplacha.2015.12.018.
Stuart, S.A., Choat, B., Martin, K.C., Holbrook, N.M., Ball, M.C., 2007. The role of freezing in setting the latitudinal limits of mangrove forests. New Phytol. 173, 576–583. https://doi.org/10.1111/j.1469-8137.2006.01938.x.
Stuiver, M., Reimer, P.J., 1993. Extended 14C database and revised CALIB radiocarbon calibration program. Radiocarbon 35 (1), 215–230. https://doi.org/10.1017/S0033822200013904.
Stuiver, M., Polach, H.A., 1977. Reporting of 14C data. Radiocarbon 19 (3), 355–363. https://doi.org/10.1017/S0033822200003672.
Sugita, S., 1994. Pollen representation of vegetation in quaternary sediments: theory and method in patchy vegetation. J. Ecol. 82, 881–897.
Toniolo, T.de F., Giannini, P.C.F., Angulo, R.J., de Souza, M.C., Pessenda, L.C.R., Spotorno-Oliveira, P., 2020. Sea-level fall and coastal water cooling during the Late Holocene in Southeastern Brazil based on vermetid bioconstructions. Mar. Geol. 428. https://doi.org/10.1016/j.margeo.2020.106281.
Urrego, L.E., Bernal, G., Polanía, J., 2009. Comparison of pollen distribution patterns in surface sediments of a Colombian Caribbean mangrove with geomorphology and vegetation. Rev. Palaeobot. Palynol. 156, 358–375. https://doi.org/10.1016/j.revpalbo.2009.04.004.

Veloso, H.P., Rangel-Filho, A.L.R., Lima, J.C.A., 1991. Classificação da Vegetação Brasileira, adaptada a um Sistema Universal. Rio de Janeiro.

Walker, R.G., 1992. facies models and modern stratigrahic concepts. In: Walker, R.G., James, N.P. (Eds.), Facies Models Response to Sea Level Change. Geological Association of Canada, Ontario, pp. 1–14.

Walsh, G.E., 1974. Mangroves: a {review}. Ecol. Halophytes 51–174. https://doi.org/10.1016/B978-0-12-586450-3.50008-1.

Wentworth, C.K., 1922. A scale of grade and class terms for clastic sediments. J. Geol. 377–392.

Woodroffe, C.D., Rogers, K., McKee, K.L., Lovelock, C.E., Mendelssohn, I.A., Saintilan, N., 2016. Mangrove sedimentation and response to relative sea-level rise. Ann. Rev. Mar. Sci. 8, 243–266. https://doi.org/10.1146/annurev-marine-122414-034025.

Xie, D., Schwarz, C., Kleinhans, M.G., Zhou, Z., van Maanen, B., 2022. Implications of coastal conditions and sea-level rise on mangrove vulnerability: a bio-morphodynamic modeling study. J. Geophys. Res. Earth Surf. 127, e2021JF006301. https://doi.org/10.1029/2021JF006301.

Xu, Q., Tian, F., Bunting, M.J., Li, Y., Ding, W., Cao, X., He, Z., 2012. Pollen source areas of lakes with inflowing rivers: modern pollen influx data from Lake Baiyangdian, China. Quat. Sci. Rev. 37, 81–91. https://doi.org/10.1016/j.quascirev.2012.01.019.

Yao, Q., Cohen, M., Liu, K., Fan, D., Rodrigues, E., Maiti, K., de Souza, A.V., Aragón-Moreno, A.A., Rohli, R., Yin, D., Pessenda, L.C.R., 2022. Mangrove expansion at poleward range limits in North and South America: late-Holocene climate variability or Anthropocene global warming? Catena (Amst) 216PB, 106413.

Yao, Q., Liu, K., 2017. Dynamics of marsh-mangrove ecotone since the mid-Holocene: a palynological study of mangrove encroachment and sea level rise in the Shark River Estuary, Florida. PLoS One 12, e0173670. https://doi.org/10.1371/journal.pone.0173670.

Yao, Q., Liu, K., Platt, W.J., Rivera-Monroy, V.H., 2015. Palynological reconstruction of environmental changes in coastal wetlands of the Florida Everglades since the mid-Holocene. Quat. Res. 83, 449–458. https://doi.org/10.1016/j.yqres.2015.03.005.

Zular, A., Utida, G., Cruz, F.W., Sawakuchi, A.O., Wang, H., Bícego, M., Giannini, P.C., Rodrigues, S.I., Garcia, G.P.B., Vuille, M., Sifeddine, A., Zocatelli, R., Mendes, V.R., Turcq, B., 2018. The effects of mid-Holocene fluvio-eolian interplay and coastal dynamics on the formation of dune-dammed lakes in NE Brazil. J. Quaternary Sci. Rev.

Further reading

Oppenheimer, M., Glavovic, B., Hinkel, J., van de Wal, R., Magnan, A.K., Abd-Elgawad, A., et al., 2019. Sea level rise and implications for low-lying islands, coasts and communities, in: H.-O. Prtner, D.C.R.V.M.-D.P.Z.M.T.E.P.& N.M.W. (Ed.), IPCC Special Report on the Ocean and Cryosphere in a Changing Climate. Cambridge University Press.